

© 2015 David Hanley

AN IMPROVED MODEL-BASED OBSERVER FOR INERTIAL  
NAVIGATION FOR QUADROTORS WITH LOW COST IMUS

BY

DAVID HANLEY

THESIS

Submitted in partial fulfillment of the requirements  
for the degree of Master of Science in Aerospace Engineering  
in the Graduate College of the  
University of Illinois at Urbana-Champaign, 2015

Urbana, Illinois

Adviser:

Professor Timothy Bretl

# ABSTRACT

In this thesis, we present a model-based observer for inertial navigation of quadrotors and other multirotor aircraft. We include in our model a Coriolis term that has been neglected in prior work. Doing so allows us to estimate the entire velocity vector in the quadrotor’s frame of reference—including along the z-axis of this frame—with data only from a low-cost inertial measurement unit (IMU), something that has not been demonstrated previously. An observability analysis predicts that our proposed observer will perform well. Experimental results over 110 flight trials verify this prediction, showing that our proposed observer achieves lower root mean square error than three other state-of-the-art model-based observers.

*To my family for their love and support.*

# ACKNOWLEDGMENTS

This thesis would not have been possible without the help of many people. First, I would like to thank my adviser, Professor Timothy Bretl for all his encouraging support and insights. Conversations with Professor Bretl always challenge my thought process and provoke growth. In addition, I would like to thank all the members of the Bretl Research Group during my time as a Master's student (Navid Aghasadeghi, Aadeel Akthar, Andy Borum, Kevin Chen, Joe DeGol, Xinke Deng, Jessica Mullins, Mary Nguyen, Jamie Norton, Jacob Wagner, and Sean Yen). Each of them make the lab a great place to work. In particular, I would like to thank Joe DeGol and Xinke Deng for their many hours of help and advice. Finally, I would like to thank my family. Their love and support has enabled me to write this thesis. This work is supported in part by the National Science Foundation Grant No. 14-46765 and 14-27111.

# TABLE OF CONTENTS

CHAPTER 1	INTRODUCTION . . . . .	1
1.1	Outline . . . . .	3
CHAPTER 2	QUADROTOR DYNAMICS . . . . .	4
2.1	Rigid Body Dynamics and the Quadrotor Airframe . . . . .	4
2.2	Propeller Aerodynamics . . . . .	6
CHAPTER 3	INERTIAL NAVIGATION TECHNOLOGY . . . . .	10
3.1	Accelerometers and Gyroscopes . . . . .	10
3.2	The Inertial Measurement Unit . . . . .	11
3.3	Performance Grades and Sensor Models . . . . .	13
CHAPTER 4	SYSTEM MODEL AND OBSERVER DESIGN . . . . .	16
4.1	Proposed Observer . . . . .	16
4.2	Previously Developed Observers . . . . .	21
4.3	Variants of Proposed Observer . . . . .	23
CHAPTER 5	OBSERVABILITY ANALYSIS . . . . .	25
5.1	Observability Rank Condition . . . . .	25
5.2	Degree of Observability . . . . .	29
CHAPTER 6	FLIGHT TESTS AND RESULTS . . . . .	33
6.1	Illustration of Observers . . . . .	33
6.2	Results Over 110 Trials . . . . .	35
CHAPTER 7	CONCLUSIONS . . . . .	41
APPENDIX A	DETAILED RESULTS . . . . .	42
REFERENCES	. . . . .	57

# CHAPTER 1

## INTRODUCTION

For several decades now, the well established navigation architecture for aerospace vehicles has been to integrate an inertial measurement unit (IMU) with an externally provided or on-board navigation aid. Typical aided navigation architectures for aerospace vehicles have integrated outputs from the inertial measurement units to produce an accurate a priori measurement that is then used in an observer that corrects errors in the inertial navigation system with the help of the aiding sensor [1]. With respect to the inertial navigation system's algorithms, much of the work over the past few decades has focused on reducing error produced through integration methods [2–5]. In particular, research on integration algorithms have focused primarily on compensating for coning and sculling motion [6–9].

For small aerial platforms, so-called low cost IMUs have been a popular choice to use in integrated navigation systems due to their small size and weight [10]. These IMUs have been used in conjunction with ultrasonic sensors and magnetometers [11], lasers [12, 13], GPS [14, 15], and monocular vision [16]. These low cost IMUs, which are typically also microelectromechanical (MEMs) sensors, are usually characterized by a worse turn-on and in-run bias stability than tactical grade and other higher grade IMUs. The turn-on and in-run scale-factor stability of low cost IMUs is typically also worse than these higher grade sensors. Finally, but not exhaustively, these IMUs have a greater sensitivity to temperature changes.

Recently, several researchers have proposed using the dynamics of multi-rotor helicopters to replace the integrated outputs of a portion of the inertial navigation system with an observer [17–21]. In typical integrated INS methods, errors propagate due to alignment errors (i.e. modeling the IMU in an incorrect frame of reference), sensor errors (i.e. various forms of bias and scale factor errors inherent to the sensors), and computational errors in the integration algorithm [1]. While these observers would actually pro-

duce worse state estimates, due to model uncertainty, than the integration methods for navigation grade or even tactical grade IMUs (given a correct initialization), the relatively large sensor errors in low cost IMUs allow these observers to outperform integrated methods. In earlier work, models of a quadrotor in perfect hover were used to estimate attitude. In particular, the accelerometers measure the specific force produced by the thrust of the rotors and this was used to obtain improved pitch and roll measurements [17]. Researchers then proposed that accelerometers in the plane of the propellers actually measure force due to the so called H-force drag. A simplified model of this force is proportional to the velocity of the vehicle in the plane of the rotors [22]. This work was originally used for control of quadrotors, but has since been used for state estimation of vehicle pitch, roll, and velocities in the plane of a quadrotor’s propellers. It has been shown how this H-force drag model improves the quality of the IMU state estimation over both integration methods and the earlier perfect hover assumption [18–20]. Methods have also been proposed to estimate both gyroscope bias and the H-force drag term on-line with only IMU data [18,19,21]. This work has also shown that using this H-force drag model performs better than previously developed models as the correcting rate from an aiding sensor degrades [20]. Researchers have studied how wind and errors in model parameters impact the attitude estimate of an IMU and magnetometer navigation system that also uses the H-force drag in its dynamic model [23].

In this thesis, we present a new observer using only measurements from a low cost IMU on-board a quadrotor. We use the H-force drag model developed in previous work, however, we also include the Coriolis effect in our model. Previous work has either completely omitted any mention of this effect [18] or has ignored it due an assumption that the term is “small enough to be neglected [19].” One justification for assuming the Coriolis effect can be safely ignored is that “the vehicle cannot translate or rotate quickly without rendering exteroceptive sensor data useless [20].” We aim to show in this thesis that the Coriolis term can be used to produce substantial improvements over current state-of-the-art observers. This term should not be ignored, because it allows the entire velocity vector in the helicopter frame to be observable, even when the vehicle is not translating or rotating quickly. Current state-of-the-art estimators cannot estimate the entire velocity vector in the helicopter frame. By using the Coriolis term, our observer can do this



and produce root mean square errors in the state estimates that are lower than state-of-the-art observers.

## 1.1 Outline

In Chapter 2, we describe the dynamics of quadrotor vehicles. Inertial sensor technology is described in Chapter 3. In Chapter 4, we present three variants of our observer and three state-of-the-art observers. The difference between these observers is in their model of multirotor helicopters and inertial measurement units. In Chapter 5, we present the nonlinear observability matrix of our proposed observer to show how the entire velocity vector is observable due to the fact that we include the Coriolis effect. We also numerically show how strong the observability properties of our proposed observer are and compare these properties to three state-of-the-art observers. In Chapter 6, we show results demonstrating the effectiveness of our proposed estimator over 110, thirty second flight trials. Chapter 7 offers conclusions and presents future work.

# CHAPTER 2

## QUADROTOR DYNAMICS

In the previous chapter, we introduced model-based observers as an alternative to integration of IMU data. We claim that these model-based observers can improve the performance of inertial navigation systems for low cost inertial sensors when compared to integration algorithms. In this chapter, we present a dynamic model of quadrotor robots as it has been presented in previous literature. This model relies on the well known theory of dynamics for rigid bodies. The forces and torques in these dynamic equations are modeled with existing work on propeller aerodynamics.

### 2.1 Rigid Body Dynamics and the Quadrotor Airframe

Consider the quadrotor system depicted in Figure 2.1. This system has two defined coordinate frames: an inertial frame ( $\mathcal{F}^W$ ) and a body frame ( $\mathcal{F}^B$ ). We wish to express the dynamics of this system in the form of

$$\dot{x} = f(x, u) \tag{2.1}$$

where system inputs  $u = \begin{bmatrix} T & \tau_x & \tau_y & \tau_z \end{bmatrix}^\top$  are the thrust ( $T$ ) and torques ( $\tau_x, \tau_y, \tau_z$ ) commanded by a controller to the system's propellers.

We treat the quadrotor as a single rigid body. It has been shown that rigid bodies have, in general, six degrees of freedom corresponding to the location and orientation of the rigid body (see, for example, [25]). We can chose to represent location and orientation in many ways. However, it is common in literature on quadrotors to use a simple Cartesian representation of position and ZYX Euler angles for orientation. The dynamics of a rigid body can be

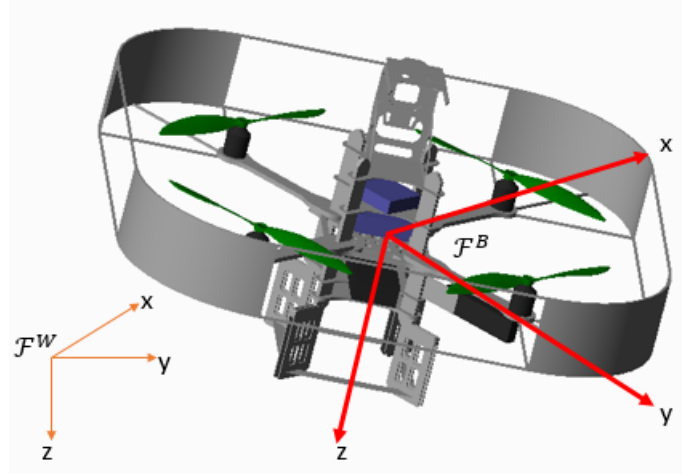


Figure 2.1: Ascending Technologies Pelican quadrotor with world and body frame [24].

described through Newton's second law and Euler's equations of motion

$$\begin{aligned} J\dot{\omega} + \hat{\omega}J\omega &= \tau \\ F &= m\dot{v} \end{aligned} \tag{2.2}$$

where  $J$  is the moment of inertia,  $\omega$  is the angular velocity vector,  $\tau$  is the torque exerted on the body,  $F$  is the force exerted on the body,  $m$  is the mass of the body, and  $v$  is the velocity of the body. To complete the equations of motion we use the kinematic relationships

$$\begin{aligned} \dot{q} &= v \\ \dot{\theta} &= S\omega \end{aligned} \tag{2.3}$$

where

$$S = \begin{bmatrix} 1 & \tan \theta_y \sin \theta_x & \tan \theta_y \cos \theta_x \\ 0 & \cos \theta_x & -\sin \theta_x \\ 0 & \frac{\sin \theta_x}{\cos \theta_y} & \frac{\cos \theta_x}{\cos \theta_y} \end{bmatrix}$$

$\theta = \begin{bmatrix} \theta_x & \theta_y & \theta_z \end{bmatrix}^T$  is the ZYX Euler angle vector, and  $q$  is the position vector.

Due to the quadrotor's symmetry, several methods exist in the literature on assumptions about the vehicles moment of inertia matrix that can be leveraged in modeling and control. It is very common to assume that the

center of gravity of the vehicle is at the origin of  $\mathcal{F}^B$  and that the products of inertia are zero [26–28]. The diagonal elements are then estimated through experiment or rough analytical estimates. Bangura and Mahony have proposed an alternative model [29]

$$\begin{aligned}
J_{xx} &= m_{cg} \frac{h_{cg}^2 + 3r_{cg}^2}{12} + 2m_m L^2 + \frac{1}{6}m_m (3r_m^2 + 4h_m^2) + \dots \\
&\quad 2m_r L^2 + \frac{1}{6}m_r (2R)^2 \\
J_{yy} &= m_{cg} \frac{h_{cg}^2 + 3r_{cg}^2}{12} + 2m_m L^2 + \frac{1}{6}m_m (3r_m^2 + 4h_m^2) + \dots \\
&\quad 2m_r L^2 + \frac{1}{6}m_r c^2 \\
J_{xy} &= J_{yx} = 0 \\
J_{zz} &= \frac{m_{cg} r_{cg}^2}{2} + 4m_m L^2 + 2m_m r_m^2 + \frac{m_r ((2R^2) + c^2)}{3} + 4m_r L^2 \\
J_{xz} &= J_{yz} = J_{zx} = J_{zy} = 2m_m h_m L + 2m_r h L
\end{aligned} \tag{2.4}$$

where  $m_{cg}$  is the mass of the quadrotor which is assumed to be cylindrical about the body z-axis with radius  $r_{cg}$  and height  $h_{cg}$ ,  $h$  is the height of each rotor above the origin,  $m_r$  is the mass of each rotor,  $R$  is the radius of each rotor,  $c$  is the chord length of the rotors,  $m_m$  is the mass of each motor,  $r_m$  is the radius of each motor,  $L$  is the length from the center of gravity to the hub of the rotor, and  $h_m$  is the height of each motor. Of course, when possible to model a vehicle sufficiently accurately using computer drafting techniques, most software available will produce an estimate of the vehicle's moment of inertia that is more accurate than any of the alternative methods.

## 2.2 Propeller Aerodynamics

Many of the aerodynamic effects of a rotor can be derived by integrating the aerodynamic force per surface increment. The lift force,  $dL$ , and drag force,  $dD$ , at a point,  $\ell$ , along the rotor blade can be expressed as

$$\begin{aligned}
dL &= \frac{1}{2} \rho U(\ell)^2 C_{L\alpha} \alpha(\ell) c d\ell \\
dD &= \frac{1}{2} \rho U(\ell)^2 (C_{D0} + C_{Di} \alpha(\ell)^2) c d\ell
\end{aligned} \tag{2.5}$$

where  $\rho$  is the air density,  $U$  is the airspeed,  $c$  is the chord,  $c dl$  is the surface increment,  $C_{L\alpha}$  is the lift coefficient,  $C_{D0}$  is the parasitic drag coefficient,  $C_{Di}$  is the lift-induced drag coefficient, and  $\alpha$  is the local angle of attack [30].

By integrating the lift per surface increment, researchers have derived an expression of the lift force produced by a rotor

$$LF = \rho c R^3 \omega_r^2 C_{L\alpha} \left( \frac{\alpha_0}{3} - \frac{\bar{w} + L(\epsilon_1 \omega_y - \epsilon_2 \omega_x)}{2R|\omega_r|} \right) \quad (2.6)$$

where  $\alpha_0$  is the rotor's average pitch angle at rest,  $\omega_r$  is the rotation speed of the rotor,  $\omega_x$  and  $\omega_y$  are the angular velocities of the quadrotor about the x and y-axes respectively,  $\bar{w}$  is the sum of the induced velocity and the wind speed in the z-axis body frame of reference subtracted by the velocity of the quadrotor in the z-axis body frame of reference, and  $\epsilon_i$  takes on value -1, 0, or 1 depending on the rotor under consideration [30]. It is common to simplify this expression as

$$LF = k_f \omega_r^2 \quad (2.7)$$

where  $k_f$  is a constant determined through experiment and  $\omega_r$  is the rotor's rotation rate [31]. In a similar manner to the lift force, the drag moment has been derived as [30]

$$\begin{aligned} DM = & -\text{sgn}(\omega_r) \rho c R^4 \omega_r^2 \left( \frac{C_{D0}}{4} + C_{Di} \alpha_0^2 \left( \frac{\alpha_0}{4} - \frac{2\bar{w}}{3R|\omega_r|} \right) \right) + \dots \\ & - \text{sgn}(\omega_r) \rho c R^4 \omega_r^2 \left( -C_{L\alpha} \frac{\bar{w}}{R|\omega_r|} \left( \frac{\alpha_0}{3} - \frac{\bar{w}}{2R|\omega_r|} \right) \right). \end{aligned} \quad (2.8)$$

As with the lift force, it is common to simplify this drag moment expression as

$$DM = k_q \omega_r^2 \quad (2.9)$$

where  $k_q$  is a constant determined through experiment [31].

Integrating the drag per surface increment produces the drag force, which has been decomposed into two parts: a parasitic drag term

$$DF_0 = \left[ \begin{array}{l} \frac{1}{2} \rho c R^2 C_{D0} (|\omega_r| \bar{u} - \text{sgn}(\omega_r) \bar{w} \omega_x) \\ \frac{1}{2} \rho c R^2 C_{D0} (|\omega_r| \bar{v} - \text{sgn}(\omega_r) \bar{w} \omega_y) \end{array} \right] \quad (2.10)$$

and an induced drag term

$$DF_i = \begin{bmatrix} \rho c R^3 C_{Di} \alpha_t \left( \frac{\bar{w}}{R^2} \bar{u} + \frac{\omega_r}{3} \omega_x \right) \\ \rho c R^3 C_{Di} \alpha_t \left( \frac{\bar{w}}{R^2} \bar{v} + \frac{\omega_r}{3} \omega_y \right) \end{bmatrix} \quad (2.11)$$

where  $\bar{u}$  and  $\bar{v}$  is the difference between the wind velocity and vehicle velocity in the body frame x and y-axes respectively and  $\alpha_t$  is the rotor blade angle of attack when taking the induced velocity into account. Typically, a third drag force, the drag due to lift force, is also derived from the lift force per section increment integration. This force is the portion of the lift force acting along the vehicle's body frame x and y-axis and is expressed as

$$DF_L = \begin{bmatrix} -\frac{1}{2} \rho c C_{L\alpha} \left( R \alpha_t \bar{w} \bar{u} + \left( \text{sgn}(\omega_r) R^2 \bar{w} - \frac{R^3 \alpha_t \omega_r}{3} \right) \omega_x \right) \\ -\frac{1}{2} \rho c C_{L\alpha} \left( R \alpha_t \bar{w} \bar{v} + \left( \text{sgn}(\omega_r) R^2 \bar{w} - \frac{R^3 \alpha_t \omega_r}{3} \right) \omega_y \right) \end{bmatrix}. \quad (2.12)$$

Finally, the moment produced by the lift force of a rotor can be derived [30]

$$LM = \begin{bmatrix} \rho c R^4 C_{L\alpha} \left( \frac{|\omega_r|}{8} \omega_x + \frac{\bar{w} \text{sgn}(\omega_r)}{4R^2} \bar{u} \right) \\ \rho c R^4 C_{L\alpha} \left( \frac{|\omega_r|}{8} \omega_y + \frac{\bar{w} \text{sgn}(\omega_r)}{4R^2} \bar{v} \right) \end{bmatrix}. \quad (2.13)$$

Note that the lift force acts along the body frame z-axis, the drag moment acts about the body frame z-axis, the drag forces all act along the body frame x and y-axes, and the lift moment acts about the body frame x and y-axes.

The above propeller model was developed by applying two dimensional incompressible flow concepts about three dimensions. Hoffmann, et al. identify three flight regimes of quadrotors: the normal working state, the vortex ring state, and the windmill brake state [32]. Bangura and Mahony include two additional flight regimes: the turbulent wake state and ground effect [29]. In the normal working state the previously presented propeller model is valid. In the vortex ring state, air circulates around the rotor blade, which significantly reduces the efficiency of the rotor. This flight regime occurs during the vertical descent of the vehicle. As the vehicle descends faster, the circulation of air around the rotor blade breaks up and enters the turbulent wake state flight regime. As the vehicle descends even faster, air flows through the rotors, which changes the transfer of power to the air. This is the windmill brake state. Finally, ground effect occurs when the aerodynamics of the vehicle is significantly influenced by the presence of the ground.

As the quadrotor moves from one point to another along the rotor plane, the advancing blade of a propeller experiences a higher effective velocity than the receding blade. This causes a changing force as a blade make a revolution about the rotor hub. The effect is called blade flapping since the difference in force will tilt the rotor plane slightly. This effect is very commonly modeled among researchers [29–32]. This effect can be modeled with the equation

$$T_{def} = T \sin \kappa_1 \quad (2.14)$$

where  $T$  is the thrust vector produced by a rotor,  $T_{def}$  is the thrust generated in the direction opposing the motion of the vehicle along the rotor plane, and  $\kappa_1$  is the angle by which the thrust vector is deflected. Blade flapping also creates a moment about the hub of the rotor. This has been modeled by Hoffmann, Huang, Waslander, and Tomlin with the equation

$$M_{bf} = \kappa_2 \kappa_1 \quad (2.15)$$

where  $\kappa_2$  is the stiffness of the blade [32].

Note that in helicopter theory, several of these drag effects are aggregated into an single term called the rotor drag or H-force drag. Martin and Salaun model this term for quadrotors using the equation

$$F_H = \omega_r \lambda V_p^\perp \quad (2.16)$$

where  $F_H$  is the H-force drag exerted on the rotor,  $\lambda$  is a constant, and  $V_p^\perp$  is the velocity along the plane of the rotor [22]. This H-force drag model is particularly important to this work, because it enables us to design effective model-based observers using inertial measurement units.

# CHAPTER 3

## INERTIAL NAVIGATION TECHNOLOGY

In the previous chapter, we presented a dynamic model of quadrotor vehicles developed in the literature. This model uses the dynamics of general rigid bodies and the aerodynamics of propellers, which describes the types of forces experienced by the quadrotor. In this chapter, we introduce inertial sensing technology. This sensing technology is typically grouped into several categories: navigation grade, tactical grade, commercial grade, and so-called low-cost inertial measurement units (IMUs). This technology can also be grouped into the method used for sensing angular velocity and specific force: ring laser gyroscopes, mechanical gyroscopes and accelerometers, vibrating beam accelerometers, resonant silicon accelerometers, and micro-machined electromechanical (MEMs) gyroscopes and accelerometers to name a few. In this work we focus on low-cost MEMs IMUs since these sensors, due to small size, small part count, and low cost, are particularly common in small unmanned aircraft such as quadrotors.

### 3.1 Accelerometers and Gyroscopes

Inertial measurement units are made up of a set of accelerometers and gyroscopes. Both sensors have been a major topic of research for decades. This research has produced a wide variety of potential sensing methods (vibratory sensors, cryogenic devices, optical sensors, etc), each serving their own niche of applications. No matter the method for sensing, the principles of accelerometers and gyroscopes remain the same. Gyroscopes are designed to measure the angular velocity of the sensor about its sensitive axis. Accelerometers measure a quantity called the specific force. Specific force is best understood by considering the accelerometer model presented in Figure 3.1. In this simple accelerometer, a mass is connected to a box through springs.



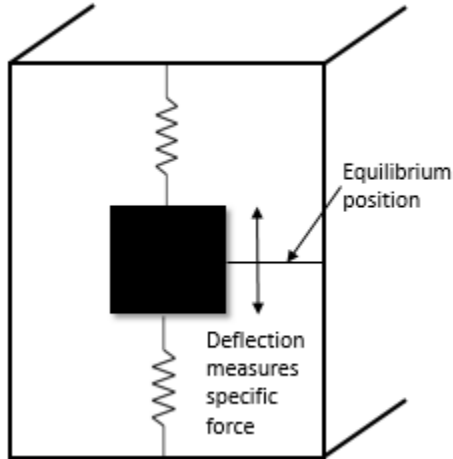


Figure 3.1: Accelerometer model [1].

The deflection of the mass, along with Hooke's law, is used to produce the output of the accelerometer. Thus when a force acts equally on the mass and its container, the sensor measures no specific force. As an example, consider an accelerometer accelerating due to gravitational force. Since gravity acts on both the mass and the container, the sensor measures zero specific force. On the other hand consider the accelerometer sitting on a table. The sensor would in this case measure the normal force exerted on the container since that force is not exerted on the mass. In short, specific force is the difference between the force experienced by the mass and its container divided by the known mass.

## 3.2 The Inertial Measurement Unit

A set of accelerometers and gyroscopes are typically configured together such that the entire specific force vector and angular velocity of a rigid body is measured. This combination of sensors is called the inertial measurement unit (IMU). Accelerometers and gyroscopes can be configured in various ways to produce an IMU. However, the most common configuration is to use a set of three accelerometers and three gyroscopes arranged such that each accelerometer measures the specific force along an axis orthogonal to the other two. Likewise, the three gyroscopes are configured so that each sensor measures the angular velocity about an axis orthogonal to the other

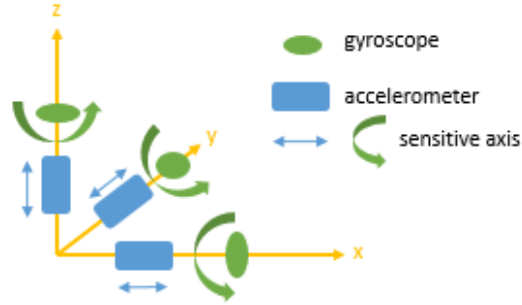


Figure 3.2: Orthogonal Arrangement of Inertial Sensors in IMU.

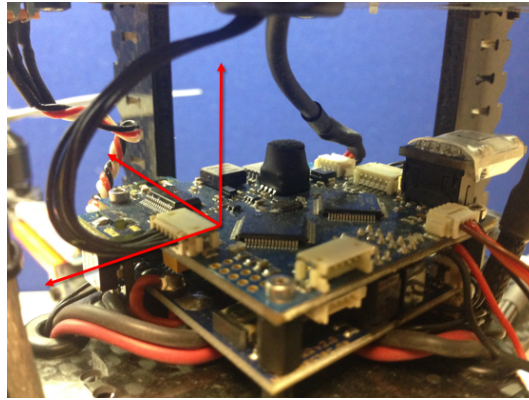


Figure 3.3: Microcontroller with Embedded IMU Onboard Pelican Quadrotor [24].

two. This orthogonal arrangement is depicted in Figure 3.2.

This orthogonal arrangement is especially common with small unmanned aircraft, since weight and size are often a priority. This orthogonal arrangement, typically leveraging low-cost MEMS inertial sensors, has no redundant sensors. Figure 3.3 shows a microcontroller with an IMU embedded on-board. It is clear from the sensitive axes of the three gyroscopes drawn on the figure that this IMU is in an orthogonal arrangement. This particular microcontroller is onboard UAVs from Ascending Technologies. The Ascending Technologies Pelican quadrotor is used in experiment in Chapter 6 of this thesis.

Of course, not all IMUs are arranged in an orthogonal configuration. Sukkarieh, Gibbens, Grocholsky, Willis, and Durrant-Whyte for example designed a low-cost inertial measurement unit (shown in Figure 3.4) for unmanned air vehicles. This truncated tetrahedron design was meant to add

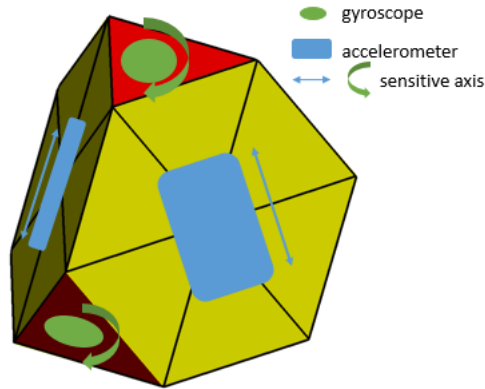


Figure 3.4: A Redundant IMU Developed for Low-Cost Inertial Sensors [33].

redundancy to the sensor, thereby enabling fault detection and greater accuracy [33].

Inertial measurement units are not simply arrangements of inertial sensors however. IMUs typically also contain electronics for the instrument power supplies, re-balancing loops, temperature monitoring, analog to digital conversion, and more. Often anti-vibration mounts are also installed on IMUs [1].

### 3.3 Performance Grades and Sensor Models

It is very common for inertial measurement units to be calibrated prior to being installed on a vehicle. By calibration, we mean the use of a wide variety of techniques to predict how the measured angular velocity vector and specific force will differ from their true values. This difference is influenced by temperature, vibration, sensor age, and magnetic fields to name a few [1]. The performance grade of an inertial measurement unit is described by contributors to errors in the sensors after calibration. Titterton and Weston propose

the following error model for describing the performance of gyroscopes

$$\begin{aligned}
e_\omega = & B_G + B_g \begin{bmatrix} a_x \\ a_y \\ a_z \end{bmatrix} + B_{ae} \begin{bmatrix} a_y a_z \\ a_z a_x \\ a_x a_y \end{bmatrix} + B_{ai} \begin{bmatrix} \omega_y \omega_z \\ \omega_z \omega_x \\ \omega_x \omega_y \end{bmatrix} + \dots \\
& S_G \begin{bmatrix} \omega_x \\ \omega_y \\ \omega_z \end{bmatrix} + M_G \begin{bmatrix} \omega_x \\ \omega_y \\ \omega_z \end{bmatrix} + w_G
\end{aligned} \tag{3.1}$$

where  $e_\omega$  is the error vector of the angular velocity measurement,  $a_x$ ,  $a_y$ , and  $a_z$  are the accelerations acting on the host vehicle,  $\omega_x$ ,  $\omega_y$ , and  $\omega_z$  are the true angular velocities applied to the vehicle,  $B_G$  is the residual fixed biases present (sometimes called turn-on bias),  $B_g$  is the g-dependent bias,  $B_{ae}$  are the anisoelastic coefficients,  $B_{ai}$  are the aniso inertia coefficients,  $S_G$  are the scale-factor errors (expressed in a diagonal matrix),  $M_G$  are cross-coupling terms (expressed in a skew symmetric matrix), and  $w_G$  are the in-run random bias errors (sometimes called random walk error). Similarly, the error model proposed for describing the performance of accelerometers is

$$e_f = B_A + B_v \begin{bmatrix} a_y a_z \\ a_z a_x \\ a_x a_y \end{bmatrix} + S_A \begin{bmatrix} a_x \\ a_y \\ a_z \end{bmatrix} + M_A \begin{bmatrix} a_x \\ a_y \\ a_z \end{bmatrix} + w_A \tag{3.2}$$

where  $e_f$  is the error vector of the specific force measurement,  $B_A$  is the residual fixed biases present (sometimes called turn-on bias),  $B_v$  are the vibro-pendulous error coefficients,  $S_A$  are the scale-factor errors (expressed in a diagonal matrix),  $M_A$  are cross-coupling terms (expressed in a skew symmetric matrix), and  $w_A$  are the in-run random bias errors (sometimes called random walk error) [1].

Based on these performance metrics, inertial measurements units have been typically divided into several grades: navigation grade, tactical grade, industrial grade, and low-cost or hobbyist grade. Naturally, IMU weight increases with improved performance, as does cost. Therefore, any designer must balance their performance needs with the weight and cost requirements of their system. While there is no standard definition of these various IMU grades, Chao, Coopmans, Di, and Chen have provided some guidelines on characteristics of each sensor grade. These guidelines are expressed in Table 3.1.

IMU Type	Navigation Grade	Tactical Grade	Industrial Grade	Low-Cost Grade
Cost (\$)	> 50k	10-20k	0.5-3k	< 500
Weight	> 5 lbs	$\approx 1$ lb	< 5 oz	< 2 oz
Gyro Bias	$< 0.1 \frac{\text{deg}}{\text{hr}}$	$0.1-10 \frac{\text{deg}}{\text{hr}}$	$< 1 \frac{\text{deg}}{\text{sec}}$	$> 1 \frac{\text{deg}}{\text{sec}}$
Gyro Random Walk	$< 0.005 \frac{\text{deg}}{\sqrt{\text{hr}}}$	$0.2-0.5 \frac{\text{deg}}{\sqrt{\text{hr}}}$	Not Available	Not Available
Accel Bias	5-10 $\mu\text{g}$	0.02-0.04 mg	$\approx 5$ mg	> 5 mg

Table 3.1: IMU Grades [10]

# CHAPTER 4

## SYSTEM MODEL AND OBSERVER DESIGN

In the previous chapter, we presented the inertial measurement unit, its components, performance characteristics, and models of the sensing technology. For small unmanned aircraft, low-cost MEMs IMUs have become the dominant inertial sensing technology. In this chapter we use a simplified model of the quadrotor and IMU to develop a model-based observer. Then, we introduce three alternative model-based observers presented in existing literature to compare our proposed observer against. Finally, we present two variants of our proposed observer to facilitate this comparison.

### 4.1 Proposed Observer

Consider the quadrotor system depicted in Figure 2.1. We define a world coordinate system ( $\mathcal{F}^W$ ) which we shall treat as an inertial frame of reference with an x-axis pointing North, y-axis pointing East, and z-axis pointing in line with the gravity vector. We define the body frame ( $\mathcal{F}^B$ ) attached to the quadrotor as shown. We assume that the x-y plane of the body frame is in the plane of the rotors, the origin of this frame is at the center of mass and is also where the IMU is located. We make these assumptions out of convenience. It is relatively straight forward to apply this work when these assumptions are not valid.

In this thesis, we use the ZYX Euler angle sequence to express the orientation of the quadrotor. The dynamics of the roll ( $\phi$ ), pitch ( $\theta$ ), and yaw ( $\psi$ ) Euler angles are expressed as

$$\begin{aligned}\dot{\phi} &= \omega_x + \omega_z \tan \theta \cos \phi + \omega_y \tan \theta \sin \phi \\ \dot{\theta} &= \omega_y \cos \phi - \omega_z \sin \phi \\ \dot{\psi} &= \omega_y \frac{\sin \phi}{\cos \theta} + \omega_z \frac{\cos \phi}{\cos \theta}\end{aligned}\tag{4.1}$$

where  $\omega_x$ ,  $\omega_y$ ,  $\omega_z$  represent the angular velocities about the x, y, and z-axis respectively.

The acceleration of a general rigid body with respect to an inertial frame written in terms of the body frame coordinate system is

$$a_{w,b}^b = \ddot{q}_{w,b}^b + 2\hat{\omega}_{w,b}^b v_{w,b}^b - \hat{\omega}_{w,b}^b \hat{\omega}_{w,b}^b q_{w,b}^b + \dot{\hat{\omega}}_{w,b}^b q_{w,b}^b \quad (4.2)$$

where  $\ddot{q}_{w,b}^b$  is the acceleration of the body frame with respect to the world frame written in terms of the body frame,  $q_{w,b}^b$  is the position vector,  $v_{w,b}^b$  is the velocity vector,  $\hat{\omega}_{w,b}^b$  represents a skew symmetric matrix of the angular velocity vector,  $\ddot{q}_{w,b}^b$  is the second time derivative of the position vector, and  $\dot{\hat{\omega}}_{w,b}^b$  is the skew symmetric matrix of the angular acceleration vector. To arrive at Equation 4.2, we begin with

$$v_{w,b}^b = R_w^b \dot{q}_{w,b}^w \quad (4.3)$$

and

$$\dot{q}_{w,b}^b = \dot{R}_w^b q_{w,b}^w + R_w^b \dot{q}_{w,b}^w. \quad (4.4)$$

By rearranging Equation 4.4, we get

$$\dot{q}_{w,b}^w = R_b^w \dot{q}_{w,b}^b - R_b^w \dot{R}_w^b q_{w,b}^w. \quad (4.5)$$

We now use the fact that

$$\dot{R}_w^b = -\hat{\omega}_{w,b}^b R_w^b \quad (4.6)$$

to conclude that

$$\dot{q}_{w,b}^w = R_b^w \dot{q}_{w,b}^b + R_b^w \hat{\omega}_{w,b}^b R_w^b q_{w,b}^w. \quad (4.7)$$

This allows us to arrive at an equation for the body frame velocity:

$$v_{w,b}^b = \dot{q}_{w,b}^w + \hat{\omega}_{w,b}^b q_{w,b}^b. \quad (4.8)$$

To derive the final acceleration equation, we begin with

$$a_{w,b}^b = R_w^b a_{w,b}^w = R_w^b \ddot{q}_{w,b}^w \quad (4.9)$$

whereby we can easily derive the equation

$$\begin{aligned} a_{w,b}^b = R_w^b \left( \dot{R}_b^w \dot{q}_{w,b}^b + R_b^w \ddot{q}_{w,b}^b + \dot{R}_b^w \hat{\omega}_{w,b}^b q_{w,b}^b \right) + \dots \\ R_w^b \left( R_b^w \dot{\hat{\omega}}_{w,b}^b q_{w,b}^b + R_b^w \hat{\omega}_{w,b}^b \dot{q}_{w,b}^b \right). \end{aligned} \quad (4.10)$$

Using the fact that

$$\dot{R}_w^b = R_w^b \hat{\omega}_{w,b}^b \quad (4.11)$$

we arrive at

$$a_{w,b}^b = 2\hat{\omega}_{w,b}^b \dot{q}_{w,b}^b + \ddot{q}_{w,b}^b + \hat{\omega}_{w,b}^b \hat{\omega}_{w,b}^b q_{w,b}^b + \dot{\hat{\omega}}_{w,b}^b q_{w,b}^b \quad (4.12)$$

Finally, by substituting Equation 4.8 into Equation 4.12, we arrive at Equation 4.2.

In this work, we neglect the last two terms of Equation 4.2, which depend on the position of the body frame with respect to the world frame written in terms of the body frame. We do this because the position of the quadrotor is not, using only an IMU, observable. This results in

$$\dot{v}_{w,b}^b = \frac{F^b}{m} + 2\hat{\omega}_{w,b}^b v_{w,b}^b \quad (4.13)$$

where  $F^b$  are the forces acting on the quadrotor written in terms of the body frame and  $m$  is the mass of the quadrotor.

We assume that gravity, thrust, and the H-force drag term developed in previous literature are the only forces acting on the quadrotor [18–20, 22]. For a single propeller rotating with angular velocity  $\omega^p$  the H-force drag has been modeled as

$$F_H = \omega_r \lambda V_p^\perp \quad (4.14)$$

where  $F_H$  is the H-force drag exerted on the rotor,  $\lambda$  is a constant, and  $V_p^\perp$  is the velocity along the plane of the rotor [22]. Previous work in IMU estimation has simplified this model by assuming the angular velocity of the rotor is approximately constant [18–20]. This results in

$$F_H = \mu V_p^\perp \quad (4.15)$$

which is the model we use in this thesis. The resulting dynamic equations of



motion are

$$\begin{aligned}
\dot{v}_x^b &= -g \sin \theta - \frac{\mu}{m} v_x^b - 2\omega_z v_y^b + 2\omega_y v_z^b \\
\dot{v}_y^b &= g \cos \theta \sin \phi - \frac{\mu}{m} v_y^b - 2\omega_x v_z^b + 2\omega_z v_x^b \\
\dot{v}_z^b &= g \cos \phi \cos \theta - \frac{T}{m} - 2\omega_y v_x^b + 2\omega_x v_y^b
\end{aligned} \tag{4.16}$$

where  $g$  is standard acceleration due to gravity,  $\mu$  is the H-force drag constant,  $T$  is the thrust produced by the quadrotor's four rotors,  $v_i^b$  is the velocity along the  $i^{th}$  axis in the body frame, and  $\dot{v}_i^b$  is the acceleration along the  $i^{th}$  axis in the body frame.

We use a simplified model of the IMU in this work. This model ignores g-dependent bias, anisoelastic, aniso inertial, cross-coupling, and vibro-pendulous errors [1]. This model is

$$\begin{aligned}
a_{m_i}^{SF} &= \lambda_{a_i} a_i^{SF} + \beta_{a_i} + w_{a_i} \\
\omega_{m_i} &= \lambda_{\omega_i} \omega_i + \beta_{\omega_i} + w_{\omega_i}
\end{aligned} \tag{4.17}$$

where  $a_{m_i}^{SF}$  is the specific force measured by the accelerometer along the  $i^{th}$  body frame axis,  $\omega_{m_i}$  is the measured angular velocity about the  $i^{th}$  body frame axis,  $\lambda_a$  and  $\lambda_\omega$  is the scale factor corrupting the true specific force,  $a^{SF}$ , and angular velocity respectively,  $\beta_a$  and  $\beta_\omega$  are (potentially time-varying) biases, and  $w_a$  and  $w_\omega$  is a zero mean white Gaussian noise term effecting the accelerometers and gyroscopes.

In our observer, we estimate roll, pitch, and the three body frame velocities. Again, to the best of our knowledge, the observer we propose is the only such observer for multirotor helicopters that can estimate the entire body frame velocity vector with only IMU measurements. We use a standard discrete time extended Kalman filter (EKF) for state estimation; however, other observers can be used as well. The algorithm of the discrete-time EKF

we use is [34]

$$\begin{aligned}
\bar{x}_t &= f(u_t, \hat{x}_{t-1}) \\
\bar{\Sigma}_t &= F_t \Sigma_{t-1} F_t^\top + R_t \\
K_t &= \bar{\Sigma}_t H_t^\top (H_t \bar{\Sigma}_t H_t^\top + Q_t)^{-1} \\
\hat{x}_t &= \bar{x}_t + K_t (y_t - h(\bar{x}_t)) \\
\Sigma_t &= (I - K_t H_t) \bar{\Sigma}_t
\end{aligned} \tag{4.18}$$

where  $f(u_t, \hat{x}_{t-1})$  is the a priori model of the evolution of the system given previous state estimates and system inputs,  $h(\bar{x}_t)$  is the observation model of the system given the a priori state  $(\bar{x}_t)$ ,  $F_t$  and  $H_t$  are the Jacobian matrices of the a priori model and the observation model respectively,  $R_t$  and  $Q_t$  are the covariance matrices of additive noise in the system model and observation model respectively,  $K_t$  is the Kalman gain at time  $t$ ,  $y_t$  is the sensor measurements at time  $t$ , and  $\Sigma_t$  is the estimated covariance of the state estimate  $(\hat{x}_t)$  at time  $t$ . The a priori model we use in the EKF is

$$\begin{aligned}
\dot{\check{\phi}} &= \omega_{m_x} + \omega_{m_z} \tan \check{\theta} \cos \check{\phi} + \omega_{m_y} \tan \check{\theta} \sin \check{\phi} \\
\dot{\check{\theta}} &= \omega_{m_y} \cos \check{\phi} - \omega_{m_z} \sin \check{\phi} \\
\dot{v}_x^b &= -g \sin \check{\theta} - \frac{\mu}{m} \check{v}_x^b - 2\omega_{m_z} \check{v}_y^b + 2\omega_{m_y} \check{v}_z^b \\
\dot{v}_y^b &= g \cos \check{\theta} \sin \check{\phi} - \frac{\mu}{m} \check{v}_y^b - 2\omega_{m_x} \check{v}_z^b + 2\omega_{m_z} \check{v}_x^b \\
\dot{v}_z^b &= g \cos \check{\phi} \cos \check{\theta} + a_{m_z}^{SF}.
\end{aligned} \tag{4.19}$$

This model uses gyroscope measurements for angular velocity, the z-axis accelerometer measurement, and current state estimates (denoted with a breve). For use in the EKF, Equation 4.19 must be discretized.

We use the accelerometer output along the body frame x and y-axes as the measurement in the innovation term of the EKF. This innovation term is

$$v = \begin{bmatrix} a_{m_x}^{SF} \\ a_{m_y}^{SF} \end{bmatrix} - \begin{bmatrix} -\frac{\mu}{m} \check{v}_x^b - 2\omega_{m_z} \check{v}_y^b + 2\omega_{m_y} \check{v}_z^b \\ -\frac{\mu}{m} \check{v}_y^b - 2\omega_{m_x} \check{v}_z^b + 2\omega_{m_z} \check{v}_x^b \end{bmatrix}. \tag{4.20}$$

As a part of the EKF algorithm, we must also take the Jacobian of the a priori model and output model about current state estimates and choose a priori and output model covariances.

## 4.2 Previously Developed Observers

We choose to compare our observer to three other observers. Beard, Leishman, and Macdonald presented two observers. They, along with Abeywardena, Kodagoda, Dissanyake, and Munasinghe, showed how using the H-force drag in a quadrotor model provides an improvement over other observers for multirotor helicopters and integration methods for low cost IMUs. To the best of our knowledge, these three observers represent the state-of-the-art INS for multirotor helicopters with low cost IMUs. The first estimator presented by Beard, Leishman, and Macdonald (which we shall call the BLM estimator) uses the a priori model

$$\begin{aligned}
\dot{\check{\phi}} &= \omega_{m_x} + \omega_{m_z} \tan \check{\theta} \cos \check{\phi} + \omega_{m_y} \tan \check{\theta} \sin \check{\phi} \\
\dot{\check{\theta}} &= \omega_{m_y} \cos \check{\phi} - \omega_{m_z} \sin \check{\phi} \\
\dot{\check{v}}_x^b &= -g \sin \check{\theta} - \frac{\mu}{m} \check{v}_x^b \\
\dot{\check{v}}_y^b &= g \cos \check{\theta} \sin \check{\phi} - \frac{\mu}{m} \check{v}_y^b
\end{aligned} \tag{4.21}$$

and the innovation term [19, 20]

$$v = \begin{bmatrix} a_{m_x}^{SF} \\ a_{m_y}^{SF} \end{bmatrix} - \begin{bmatrix} -\frac{\mu}{m} \check{v}_x^b \\ -\frac{\mu}{m} \check{v}_y^b \end{bmatrix}. \tag{4.22}$$

Beard, Leishman, and Macdonald, as an alternative to the BLM estimator, also present an observer that can estimate the H-force drag coefficient as a state parameter in the observer. These researchers show that this drag coefficient is observable as long as the helicopter is experiencing an acceleration in the plane of the rotors. They claim that this observer (which we shall call the BLM- $\mu$  observer) allows the user to avoid using complicated parameter identification techniques and expensive motion capture systems [19]. The

BLM- $\mu$  observer uses the a priori model

$$\begin{aligned}
\dot{\check{\phi}} &= \omega_{m_x} + \omega_{m_z} \tan \check{\theta} \cos \check{\phi} + \omega_{m_y} \tan \check{\theta} \sin \check{\phi} \\
\dot{\check{\theta}} &= \omega_{m_y} \cos \check{\phi} - \omega_{m_z} \sin \check{\phi} \\
\dot{\check{v}}_x^b &= -g \sin \check{\theta} - \frac{\check{\mu}}{m} \check{v}_x^b \\
\dot{\check{v}}_y^b &= g \cos \check{\theta} \sin \check{\phi} - \frac{\check{\mu}}{m} \check{v}_y^b \\
\dot{\check{\mu}} &= 0
\end{aligned} \tag{4.23}$$

and the innovation term [19]

$$v = \begin{bmatrix} a_{m_x}^{SF} \\ a_{m_y}^{SF} \end{bmatrix} - \begin{bmatrix} -\frac{\check{\mu}}{m} \check{v}_x^b \\ -\frac{\check{\mu}}{m} \check{v}_y^b \end{bmatrix}. \tag{4.24}$$

Both the BLM and BLM- $\mu$  observers assume that the gyroscopes measure the angular velocities exactly. Abeywardena, Kodagoda, Dissanyake, and Munasinghe attempt to estimate gyroscope bias about the x and y-axes, in addition to the states estimated by the BLM observer, to improve the performance of their estimator. The a priori model of this observer (which we shall call the AKDM observer) is

$$\begin{aligned}
\dot{\check{\phi}} &= \omega_{m_x} - \check{\beta}_{\omega_x} + \omega_{m_z} \tan \check{\theta} \cos \check{\phi} + (\omega_{m_y} - \check{\beta}_{\omega_y}) \tan \check{\theta} \sin \check{\phi} \\
\dot{\check{\theta}} &= (\omega_{m_y} - \check{\beta}_{\omega_y}) \cos \check{\phi} - \omega_{m_z} \sin \check{\phi} \\
\dot{\check{v}}_x^b &= -g \sin \check{\theta} - \frac{\mu}{m} \check{v}_x^b \\
\dot{\check{v}}_y^b &= g \cos \check{\theta} \sin \check{\phi} - \frac{\mu}{m} \check{v}_y^b \\
\dot{\check{\beta}}_{\omega_x} &= -\frac{\check{\beta}_{\omega_x}}{\tau_{\omega_x}} \\
\dot{\check{\beta}}_{\omega_y} &= -\frac{\check{\beta}_{\omega_y}}{\tau_{\omega_y}}
\end{aligned} \tag{4.25}$$

and the innovation term is

$$v = \begin{bmatrix} a_{m_x}^{SF} \\ a_{m_y}^{SF} \end{bmatrix} - \begin{bmatrix} -\frac{\mu}{m} \check{v}_x^b \\ -\frac{\mu}{m} \check{v}_y^b \end{bmatrix} \tag{4.26}$$

where  $\tau_{\omega_x}$  and  $\tau_{\omega_y}$  are the time constants of the gyroscope biases [18]. We

shall use these three observers, the BLM, BLM- $\mu$ , and AKDM, as references against which to compare our proposed observer.

### 4.3 Variants of Proposed Observer

In order facilitate comparison between our proposed observer and the BLM, BLM- $\mu$ , and AKDM observers, we present two variants of our proposed observer: the proposed- $\mu$  variant and the proposed- $\beta$  variant. Our proposed- $\mu$  observer attempts to estimate the H-force drag term as an additional state parameter. The a priori model of this estimator is

$$\begin{aligned}
\dot{\check{\phi}} &= \omega_{m_x} + \omega_{m_z} \tan \check{\theta} \cos \check{\phi} + \omega_{m_y} \tan \check{\theta} \sin \check{\phi} \\
\dot{\check{\theta}} &= \omega_{m_y} \cos \check{\phi} - \omega_{m_z} \sin \check{\phi} \\
\dot{\check{v}}_x^b &= -g \sin \check{\theta} - \frac{\check{\mu}}{m} \check{v}_x^b - 2\omega_{m_z} \check{v}_y^b + 2\omega_{m_y} \check{v}_z^b \\
\dot{\check{v}}_y^b &= g \cos \check{\theta} \sin \check{\phi} - \frac{\check{\mu}}{m} \check{v}_y^b - 2\omega_{m_x} \check{v}_z^b + 2\omega_{m_z} \check{v}_x^b \\
\dot{\check{v}}_z^b &= g \cos \check{\phi} \cos \check{\theta} + a_{m_z}^{SF} \\
\dot{\check{\mu}} &= 0
\end{aligned} \tag{4.27}$$

and the innovation term is

$$v = \begin{bmatrix} a_{m_x}^{SF} \\ a_{m_y}^{SF} \end{bmatrix} - \begin{bmatrix} -\frac{\check{\mu}}{m} \check{v}_x^b - 2\omega_{m_z} \check{v}_y^b + 2\omega_{m_y} \check{v}_z^b \\ -\frac{\check{\mu}}{m} \check{v}_y^b - 2\omega_{m_x} \check{v}_z^b + 2\omega_{m_z} \check{v}_x^b \end{bmatrix}. \tag{4.28}$$

Our proposed- $\beta$  observer attempts to estimate the gyroscope bias terms as an additional state parameter. The a priori model of this estimator is

$$\begin{aligned}
\dot{\check{\phi}} &= \omega_{m_x} - \check{\beta}_{\omega_x} + \omega_{m_z} \tan \check{\theta} \cos \check{\phi} + (\omega_{m_y} - \check{\beta}_{\omega_y}) \tan \check{\theta} \sin \check{\phi} \\
\dot{\check{\theta}} &= (\omega_{m_y} - \check{\beta}_{\omega_y}) \cos \check{\phi} - \omega_{m_z} \sin \check{\phi} \\
\dot{\check{v}}_x^b &= -g \sin \check{\theta} - \frac{\mu}{m} \check{v}_x^b - 2\omega_{m_z} \check{v}_y^b + 2(\omega_{m_y} - \check{\beta}_{\omega_y}) \check{v}_z^b \\
\dot{\check{v}}_y^b &= g \cos \check{\theta} \sin \check{\phi} - \frac{\mu}{m} \check{v}_y^b - 2(\omega_{m_x} - \check{\beta}_{\omega_x}) \check{v}_z^b + 2\omega_{m_z} \check{v}_x^b \\
\dot{\check{v}}_z^b &= g \cos \check{\phi} \cos \check{\theta} + a_{m_z}^{SF}
\end{aligned} \tag{4.29}$$

$$\begin{aligned}\dot{\check{\beta}}_{\omega_x} &= 0 \\ \dot{\check{\beta}}_{\omega_y} &= 0\end{aligned}$$

and the innovation term is

$$v = \begin{bmatrix} a_{m_x}^{SF} \\ a_{m_y}^{SF} \end{bmatrix} - \begin{bmatrix} -\frac{\mu}{m}\check{v}_x^b - 2\omega_{m_z}\check{v}_y^b + 2\left(\omega_{m_y} - \check{\beta}_{\omega_y}\right)\check{v}_z^b \\ -\frac{\mu}{m}\check{v}_y^b - 2\left(\omega_{m_x} - \check{\beta}_{\omega_x}\right)\check{v}_z^b + 2\omega_{m_z}\check{v}_x^b \end{bmatrix}. \quad (4.30)$$

In the proposed- $\beta$  model, we assume the bias term is constant. Abeywardena, Kodagoda, Dissanayake, and Munasinghe do not provide a means by which they estimate their time constants, so we simply omit them in our proposed- $\beta$  observer and take the limit as the time constant goes to infinity in the AKDM observer. Note again that our proposed observer, and its variants, estimate the entire velocity vector in the body frame of reference. The BLM, BLM- $\mu$ , and AKDM observers estimate only two of the three elements of this velocity vector. As we will show, this difference will cause our proposed estimator to substantially outperform our benchmark estimators. In the next chapter, we shall study the observability properties of the BLM, BLM- $\mu$ , AKDM, and the proposed observer and its variants. In Chapter 5, we shall present metrics by which we will compare these estimators and we shall show how our proposed estimator outperforms its benchmark observers.

# CHAPTER 5

## OBSERVABILITY ANALYSIS

In the previous chapter, we developed a model-based observer that includes the Coriolis term in its model. We then presented three alternative models described in previous work and two additional variants of the observer we developed to facilitate comparison with the alternative observers. In this chapter we begin the comparison with a study of the observability properties of these six models. It is obvious that using even the simplified accelerometer and gyroscope model presented in Equation 4.17 implies that all the models presented would, in fact, be technically unobservable. This is due to the fact that there exists an unknown scale factor and time varying unknown bias term for every measurement. Previous work uses simplified models of the IMU to show observability with the assumption that observers are robust to these small disturbances. We begin by exploring the use of the observability rank condition with our observer as done in previous work. We find this method rather lacking, however, because it does not indicate how easy it is to observe a system. We use two metrics presented by Krener and Ide to measure the strength of the observability of the proposed estimators [35]. From these metrics we believe the performance of the estimators can be inferred even in the presence of small disturbances. Alternatively, we could have used a sensitivity analysis similar to that presented by Hernandez, Tsotsos, and Soatto for vision-aided inertial navigation systems to find a bound on the set of indistinguishable state trajectories [36].

### 5.1 Observability Rank Condition

Previous work on observability analysis for this type of system used the observability rank condition to establish which states are locally, weakly observable when the quadrotor is near its hover condition [19, 20]. This type of

rank condition states that a nonlinear system described by

$$\begin{aligned} \dot{x} &= f(x, u), \quad x \in \mathbb{R}^n, u \in \mathbb{R}^m \\ y &= g(x), \quad y \in \mathbb{R}^p \end{aligned} \quad (5.1)$$

and observability matrix defined by

$$\mathcal{O} = \begin{bmatrix} dg(x) \\ \vdots \\ dL_f^k(g)(x) \end{bmatrix} \quad (5.2)$$

where  $dL_f^k(g)(x) = dL_f^{k-1}(g)(x)f(x, u)$ ,  $dL_f^0(g)(x) = dg(x)$ ,  
and  $dg(x) = \frac{\partial g}{\partial x}(x)$

is locally, weakly observable if the rank of the observability matrix is equal to the number of states ( $n$ ) [37]. Note that for real analytic systems, this observability rank condition is a necessary and sufficient condition for observability.

We have computed the first four rows of the observability matrix for the BLM observer as

$$\mathcal{O}_{BLM} = \begin{bmatrix} 0 & 0 & -\frac{\mu}{m} & 0 \\ 0 & 0 & 0 & -\frac{\mu}{m} \\ 0 & \frac{g\mu \cos \theta}{m} & \frac{\mu^2}{m^2} & 0 \\ -\frac{g\mu \cos \phi \cos \theta}{m} & \frac{g\mu \sin \phi \sin \theta}{m} & 0 & \frac{\mu^2}{m^2} \end{bmatrix}. \quad (5.3)$$

From this subset of the observability matrix, it is can be inferred that the BLM system is observable everywhere except where  $\phi = \frac{\pi}{2}$  or  $\theta = \frac{\pi}{2}$  since the first column of the fourth row element will be zero. However, we cannot prove that without the full observability matrix. Next we computed the first five rows of the observability matrix for the BLM- $\mu$  observer. This matrix is

$$\mathcal{O}_{BLM-\mu} = \begin{bmatrix} 0 & 0 & -\frac{\mu}{m} & 0 & -\frac{v_x}{m} \\ 0 & 0 & 0 & -\frac{\mu}{m} & -\frac{v_y}{m} \\ 0 & \frac{g\mu \cos \theta}{m} & \frac{\mu^2}{m^2} & 0 & \mathcal{O}_{(3,5)} \\ -\frac{g\mu \cos \phi \cos \theta}{m} & \frac{g\mu \sin \phi \sin \theta}{m} & 0 & \frac{\mu^2}{m^2} & \mathcal{O}_{(4,5)} \\ \mathcal{O}_{(5,1)} & \mathcal{O}_{(5,2)} & -\frac{\mu^3}{m^3} & 0 & \mathcal{O}_{(5,5)} \end{bmatrix} \quad (5.4)$$



where

$$\begin{aligned}
\mathcal{O}_{(3,5)} &= \frac{\mu v_x}{m^2} - \frac{-\frac{\mu v_x}{m} - g \sin \theta}{m} \\
\mathcal{O}_{(4,5)} &= \frac{\mu v_y}{m^2} - \frac{-\frac{\mu v_y}{m} + g \cos \theta \sin \phi}{m} \\
\mathcal{O}_{(5,1)} &= \frac{g \mu \cos \theta (-\omega_z \cos \phi - \omega_y \sin \phi)}{m} \\
\mathcal{O}_{(5,2)} &= -\frac{g \mu^2 \cos \theta}{m^2} - \frac{g \mu (\omega_y \cos \phi - \omega_z \sin \phi) \sin \theta}{m} \\
\mathcal{O}_{(5,5)} &= -\frac{\mu^2 v_x}{m^3} + \frac{g \cos \theta (\omega_y \cos \phi - \omega_z \sin \phi)}{m} + \frac{2\mu (-\frac{\mu v_x}{m} - g \sin \theta)}{m^2}.
\end{aligned} \tag{5.5}$$

From this matrix, it appears that there may be several unobservable modes. For example, when  $\omega_x$  and  $\omega_y$  are zero and  $\phi = \frac{\pi}{2}$  or  $\theta = \frac{\pi}{2}$ . Another unobservable state is when  $\phi = 0$ ,  $\theta = \frac{\pi}{2}$ , and  $\omega_y = 0$ . Again, while we can hypothesize that these may be unobservable states, we would need the full observability matrix to prove this is true. Beard, Leishman, and Macdonald presented a similar analysis where they claimed that the system becomes unobservable when the acceleration along the plane of the rotors become zero [19]. Next we computed the first six rows of the observability matrix for the AKDM observer. This matrix is

$$\mathcal{O}_{AKDM} = \begin{bmatrix} 0 & 0 & -\frac{\mu}{m} & 0 & 0 & 0 \\ 0 & 0 & 0 & -\frac{\mu}{m} & 0 & 0 \\ 0 & \frac{g \mu \cos \theta}{m} & \frac{\mu^2}{m^2} & 0 & 0 & 0 \\ -\frac{g \mu \cos \phi \cos \theta}{m} & \frac{g \mu \sin \phi \sin \theta}{m} & 0 & \frac{\mu^2}{m^2} & 0 & 0 \\ \mathcal{O}_{(5,1)} & \mathcal{O}_{(5,2)} & -\frac{\mu^3}{m^3} & 0 & -\frac{\mu^2}{m^2} & -\frac{g \mu \cos \phi \cos \theta}{m} \\ \mathcal{O}_{(6,1)} & \mathcal{O}_{(6,2)} & 0 & -\frac{\mu^3}{m^3} & \frac{g \mu \cos \phi \cos \theta}{m} & 0 \end{bmatrix} \tag{5.6}$$

where

$$\begin{aligned}
\mathcal{O}_{(5,1)} &= -\frac{g \mu \cos \theta (\omega_z \cos \phi + (-\beta_y + \omega_y) \sin \phi)}{m} \\
\mathcal{O}_{(5,2)} &= \frac{g \mu (-\mu \cos \theta + m ((\beta_y - \omega_y) \cos \phi + \omega_z \sin \phi) \sin \theta)}{m^2} \\
\mathcal{O}_{(6,1)} &= \frac{g \mu \cos \theta (\mu \cos \phi + m (-\beta_x + \omega_x) \sin \phi)}{m^2} \\
\mathcal{O}_{(6,2)} &= -\frac{g \mu (m \omega_z \cos \theta + (m (\beta_x - \omega_x) \cos \phi + \mu \sin \phi) \sin \theta)}{m^2}.
\end{aligned}$$

Finally, we computed the first five rows of our proposed observer's observability matrix as

$$\mathcal{O}_{prop} = \begin{bmatrix} 0 & 0 & -\frac{\mu}{m} & -2\omega_z & 2\omega_y \\ 0 & 0 & 2\omega_z & -\frac{\mu}{m} & -2\omega_x \\ \mathcal{O}_{(3,1)} & \mathcal{O}_{(3,2)} & \frac{\mu^2}{m^2} - 4\omega_z^2 & \frac{4\mu\omega_z}{m} & -\frac{2\mu\omega_y}{m} + 4\omega_x\omega_z \\ \mathcal{O}_{(4,1)} & \mathcal{O}_{(4,2)} & -\frac{4\mu\omega_z}{m} & \frac{\mu^2}{m^2} - 4\omega_z^2 & \frac{2\mu\omega_x}{m} + 4\omega_y\omega_z \\ \mathcal{O}_{(5,1)} & \mathcal{O}_{(5,2)} & \mathcal{O}_{(5,3)} & \mathcal{O}_{(5,4)} & \mathcal{O}_{(5,5)} \end{bmatrix} \quad (5.7)$$

where

$$\begin{aligned} \mathcal{O}_{(3,1)} &= -2g\omega_z \cos \phi \cos \theta - 2g\omega_y \cos \theta \sin \phi \\ \mathcal{O}_{(3,2)} &= \frac{g\mu \cos \theta}{m} - 2g\omega_y \cos \phi \sin \theta + 2g\omega_z \sin \phi \sin \theta \\ \mathcal{O}_{(4,1)} &= -\frac{g\mu \cos \phi \cos \theta}{m} + 2g\omega_x \cos \theta \sin \phi \\ \mathcal{O}_{(4,2)} &= -2g\omega_z \cos \theta + 2g\omega_x \cos \phi \sin \theta + \frac{g\mu \sin \phi \sin \theta}{m} \\ \mathcal{O}_{(5,1)} &= -\frac{g \cos \theta ((2m\omega_x\omega_y - 3\mu\omega_z) \cos \phi + (-\mu\omega_y + 2m\omega_x\omega_z) \sin \phi)}{m} \\ \mathcal{O}_{(5,2)} &= \frac{-g (\mu^2 + 2m^2 (\omega_y^2 - \omega_z^2)) \cos \theta}{m^2} + \dots \\ &\quad \frac{gm ((\mu\omega_y - 2m\omega_x\omega_z) \cos \phi + (2m\omega_x\omega_y - 3\mu\omega_z) \sin \phi) \sin \theta}{m^2} \\ \mathcal{O}_{(5,3)} &= \frac{8\mu\omega_z^2 - \mu \left( \frac{\mu^2}{m^2} - 4\omega_z^2 \right)}{m} \\ \mathcal{O}_{(5,4)} &= -\frac{4\mu^2\omega_z}{m^2} - 2\omega_z \left( \frac{\mu^2}{m^2} - 4\omega_z^2 \right) \\ \mathcal{O}_{(5,5)} &= -\frac{8\mu\omega_x\omega_z}{m} + 2\omega_y \left( \frac{\mu^2}{m^2} - 4\omega_z^2 \right). \end{aligned}$$

The proposed- $\mu$  and proposed- $\beta$  observability matrices have been omitted here due to their length. We find the analysis of these estimators with observability matrices insufficient for comparison. First, none of the matrices presented display the full observability matrix of a system. The rank condition generally only indicates whether or not the system is observable. The analysis we presented may allow us to infer what some unobservable modes may be, but we cannot guarantee that this is actually the case. In particular, we may identify some observable modes as unobservable. Finally, we have no indication with the observability rank condition how easy it will be for an

observer to accurately estimate the states of a system.

In the following chapter, we use two measures of the degree of observability presented in previous literature and use them to compare the six observers. These measurements use the singular values of the observability Gramian about a nominal trajectory. Recall that we claim including the Coriolis term in our proposed model allows the entire velocity vector to become observable in the body frame. Also, we can infer (through substitution), from Equation 5.7 that the proposed observer experiences an unobservable mode when  $\omega_x$ ,  $\omega_y$ , and  $\omega_z$  is zero. We also infer from Equation 5.7 that the observability of the system is not dependent on the thrust produced by the quadrotor over some time interval. These inferences will be used to establish nominal trajectories.

## 5.2 Degree of Observability

We shall use the so-called local unobservability index and local estimation condition number to assess observability. Since the observability rank condition does not imply how hard it is to observe the system, we use these metrics to allow us to make better conclusions about the observability properties of the system. The local unobservability index is defined as the reciprocal of the smallest local singular value of the local observability gramian defined as

$$P(x^0) = \int_0^{t_f} \Phi^T(t) G^T(t) G(t) \Phi(t) dt \quad (5.8)$$

where

$$G(t) = \frac{\partial g}{\partial x}(x^0(t))$$

$t_f$  is the final time, and  $\Phi$  is the fundamental matrix of the system linearized about a nominal trajectory. This local unobservability index measures how difficult it is to observe the initial state from the system's outputs. The local estimation condition number is defined as the ratio of the largest local singular value to the smallest local singular value and is a measure of how much a small change in the initial condition of one state effects the change in the output relative to small changes in the initial conditions of other states. In other words, it becomes more challenging to design an effective observer as the local unobservability index and the local estimation condition number

grows [35].

In this thesis, we compute the local observability gramian numerically. First, we choose a nominal trajectory and a small scalar  $\rho > 0$ . Then, we compute perturbed trajectories as described (using the notation presented by Kang, Krener, Xiao, and Xu) in

$$\begin{aligned}\dot{x}^\pm(t) &= f(x^\pm(t), u(t)) \\ x^\pm(0) &= x_0 \pm \rho v_i\end{aligned}\tag{5.9}$$

where the set of vectors  $v_1, v_2, \dots, v_n$  form an orthonormal basis in  $\mathbb{R}^n$ . Finally, we compute the local observability gramian with [38]

$$P_{ij} = \int_0^{t_f} \Delta_i^T(t) \Delta_j(t) dt \tag{5.10}$$

where

$$\Delta_i(t) = \frac{1}{2\rho} (g(x^+(t)) - g(x^-(t))).$$

Note that as  $\rho \rightarrow 0$  the numerical approximation approaches the true local observability Gramian. Note that when one or more of the singular values of this observability Gramian is zero, this system is unobservable.

We now compare the observability properties of the BLM, BLM- $\mu$ , and AKDM observers with the proposed observer and its variants. In our rank condition analysis, we found that the observability of our system is not directly dependent on the thrust produced by the system, but our proposed observer and its variants are dependent on the angular velocities. Therefore, we produce nominal trajectories by beginning with an initial state (all states zero except for  $\mu$  which we choose as 0.8281), setting thrust equal to the weight of the quadrotor, and then varying the angular velocity about each axis according to the function

$$\omega_i = \epsilon \sin(1.25t) \quad \text{where } i = x, y, z. \tag{5.11}$$

One way to interpret Equation 5.11 is as a deterministic model of a disturbance the quadrotor may experience in hover. We plot the unobservability index as a function of  $\epsilon$  for  $\rho = 0.0001$  in Figure 5.1. First, note that for all  $\epsilon > 0$ , all proposed systems are observable. The observability properties of the BLM and AKDM observers appear to be independent of  $\epsilon$ . Addition-

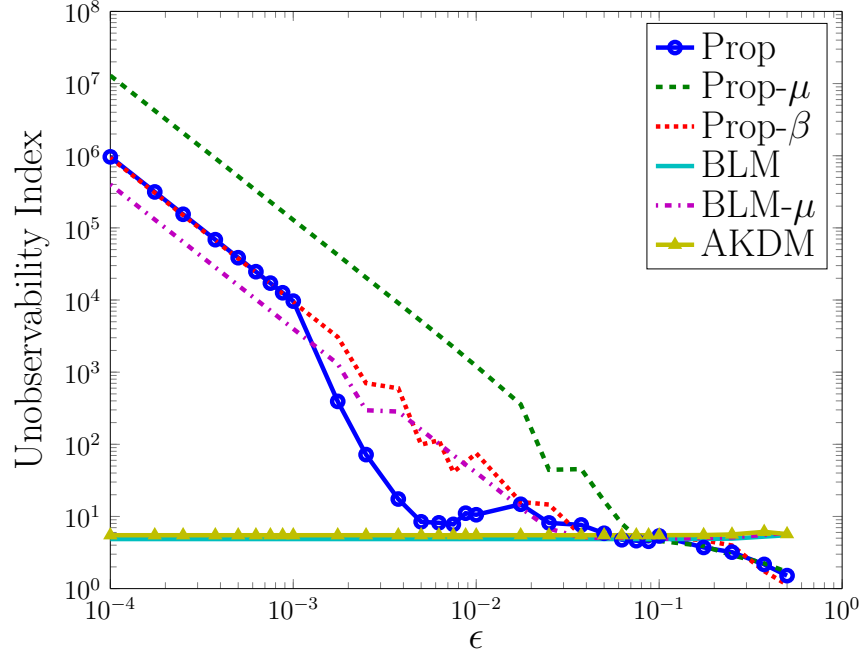


Figure 5.1: Comparison of unobservability index for six different observers. Here  $\epsilon$  is the amplitude of the angular velocity of the vehicle as described in Equation 5.11

ally, all observers appear to converge to the same unobservability index near  $\epsilon = 0.1$ . The proposed estimator appears to have a high unobservability index until approximately  $\epsilon = 0.001$  when it begins to drop rapidly relative to the BLM- $\mu$ , proposed- $\beta$ , and proposed- $\mu$  observers. The condition number (shown in Figure 5.2) for the proposed- $\beta$  estimator is consistently higher than the alternative estimators. The AKDM condition number is consistently at least two orders of magnitude larger than the BLM observer. The AKDM also appears to have a larger condition number than the proposed, BLM- $\mu$ , and proposed- $\mu$  observers for  $\epsilon > 0.01$ .

As mentioned previously, the inherent advantage of our proposed observer and its variants is the potential for the entire velocity vector to be accurately estimated. As shown, this can only happen if the angular velocities are high enough during any flight conditions the quadrotor may experience such that an observer can be used to accurately estimate the states of the quadrotor. In Chapter 6, we will evaluate these observers over 110, thirty second flight trials and discuss these results in the context of their observability properties.

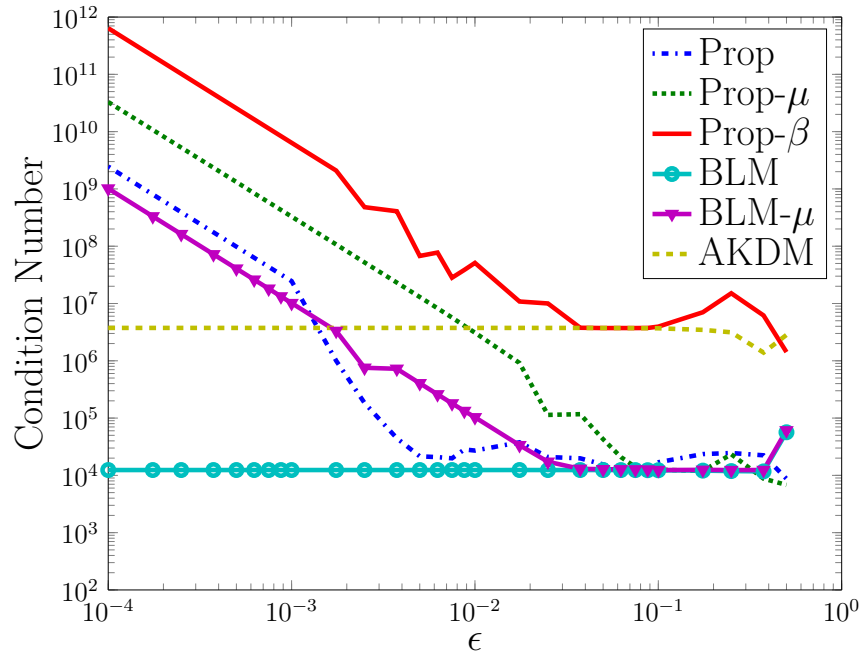


Figure 5.2: Comparison of estimation condition number for six different observers. Here  $\epsilon$  is the amplitude of the angular velocity of the vehicle as described in Equation 5.11

# CHAPTER 6

## FLIGHT TESTS AND RESULTS

In the previous section, we compared the observability properties of the six observers. In this section, we implement these observers in flight tests. These observability properties provide context to these results and some degree of explanatory power. Flight tests were conducted on an Ascending Technologies Pelican quadrotor [24]. Accelerometer and gyroscope data was collected along with position and orientation from a set of 24 Flex 3 Optitrack motion capture cameras with a roughly 100 Hz frame rate over 13 manual flights. Pairs of these cameras (one approximately 2 feet below the other) were distributed around a 40 ft  $\times$  30 ft  $\times$  9 ft room. An overview of the hardware setup is depicted in Figure 6.1. An onboard Ascending Technologies Mastermind computer collects IMU data from the vehicle’s microcontroller. Ascending Technologies claims that this IMU data is calibrated. Therefore, the remaining errors in the IMU output can be described using Equations 3.1 and 3.2. Position and orientation data is also recorded on the Mastermind computer from a wireless connection to an offboard computer that processes the Optitrack data. The offboard and onboard computers have their clocks synced using network time protocol (NTP). These thirteen flights are broken into 110, 30 second trials. We estimate the H-force drag off-line for all thirteen flights and average the results over all data points. The H-force drag was estimated to be 0.8281. We first present an illustration of our results for one trial and then present the aggregated root mean square error results for all 110 trials.

### 6.1 Illustration of Observers

Figure 6.2 shows the absolute value of the error in the estimate of velocity along the body frame z-axis in both the integrated case and for the pro-

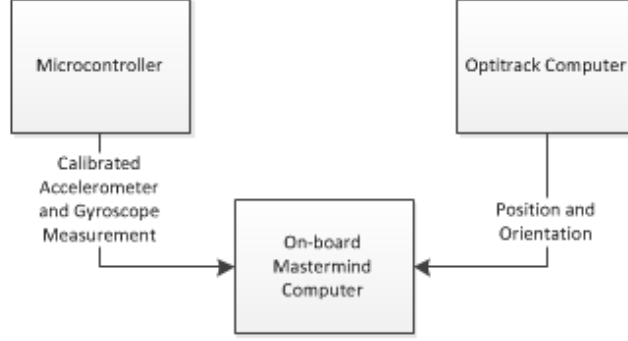


Figure 6.1: Hardware Setup

posed estimator. Note that for the BLM, BLM- $\mu$ , and AKDM observers, the body frame z-axis velocity must be computed by integrating accelerometer measurements and compensating for gravity. The improvement the proposed estimator provides is obvious. While the error in the proposed estimator is not zero, it is better: even for very short time scales. For this particular trial, the RMS error of velocity along the body frame z-axis is 0.1147 meters per second for the proposed estimator. Meanwhile, the RMS error of velocity along the body frame x and y-axes are 0.3155 and 0.3783 meters per second respectively for the proposed estimator.

Figure 6.3 also shows substantial improvements in the position estimate of the quadrotor over a 30 second period caused by the proposed estimator versus the BLM observer. Here the norm of the error in the position estimate with the proposed observer is approximately 100 meters smaller over thirty seconds than with the BLM estimator. The true positions of the quadrotor over this trial are shown in Figure 6.4. This result is due to the substantial improvement in the body frame z-axis velocity estimate, whose error is almost eight meters per second smaller in the proposed estimator after thirty seconds than with the BLM estimator. While we only show these results for one trial, these results are reflective of what we see over the 110 trials as a whole.

Figure 6.5 shows the position estimates for the BLM- $\mu$  and proposed- $\mu$  estimators together. For most of the flight, the proposed- $\mu$  estimator's position error norm grows at a much slower rate than the BLM- $\mu$ . As with the proposed estimator, this is due to the fact that we can leverage the Coriolis effect to estimate the body frame Z velocity. Toward the end of the flight, however, the proposed- $\mu$  observer has a very sudden growth in



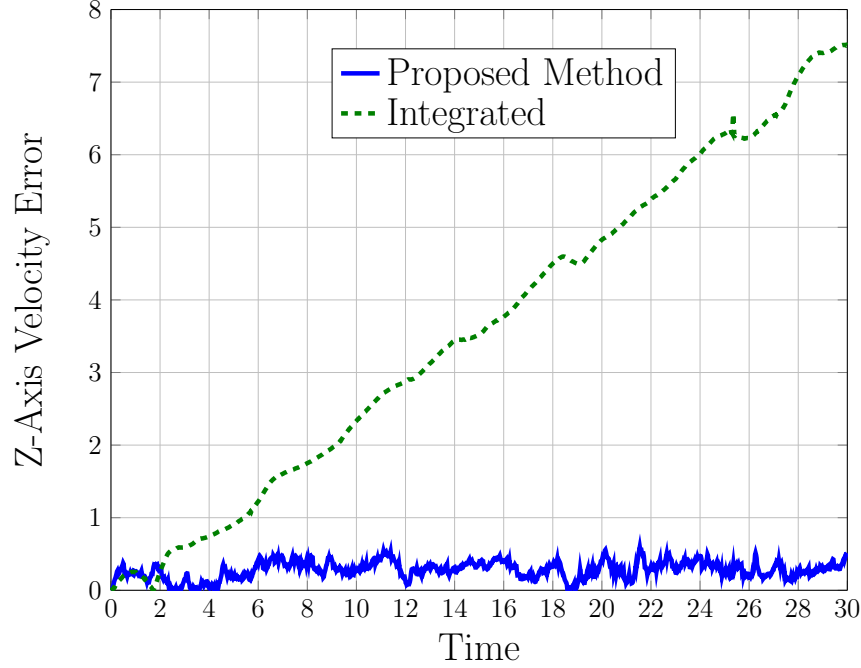


Figure 6.2: Error Along Body Frame z-Axis

its position error norm. The results from both the BLM- $\mu$  and proposed- $\mu$  observers are much less consistent across the 110 trials than the BLM and proposed estimators' results. Figure 6.6 shows the norm of the position error for the BLM- $\mu$  and proposed- $\mu$  observers for a different trial. These results are quite different from 6.5 since the proposed- $\mu$  position error is significantly smaller than the BLM- $\mu$  error after thirty seconds.

Figure 6.7 compares the norm of the position error of the AKDM observer with the proposed- $\beta$  estimate. Again the norm of the error in the position estimate with the proposed- $\beta$  observer is approximately 100 meters smaller over thirty seconds than with the AKDM estimator. Like with the results from Figure 6.3 this result is due to the substantial improvement in the body frame z-axis velocity estimate.

## 6.2 Results Over 110 Trials

We aggregate the results for 110, thirty second trials into the following tables: Table 6.1 shows the average root mean square (RMS) error for each estimator over 110 cases, Tables 6.2 and 6.3 present the maximum and minimum RMS

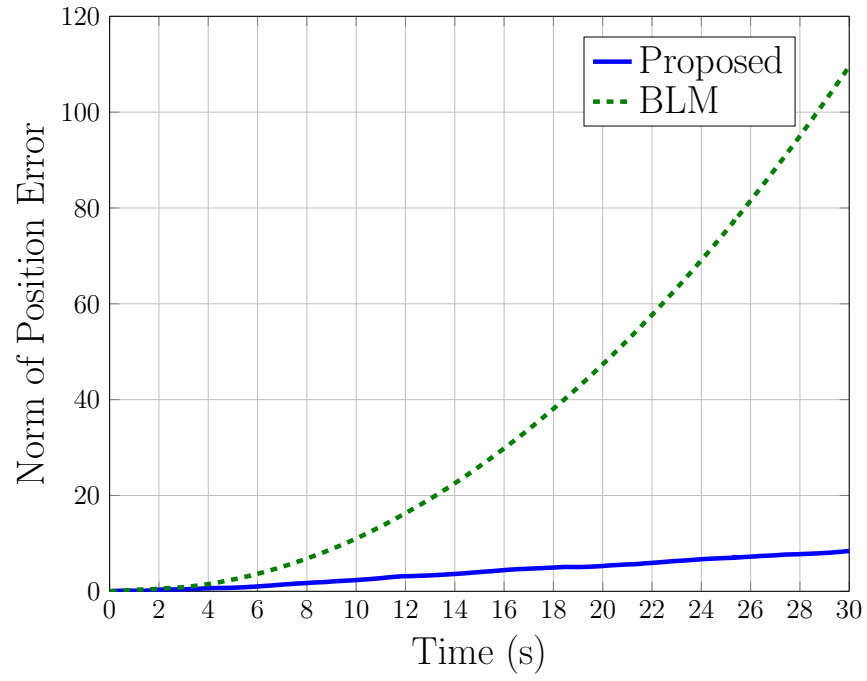


Figure 6.3: Error in Position of BLM and Proposed Estimator

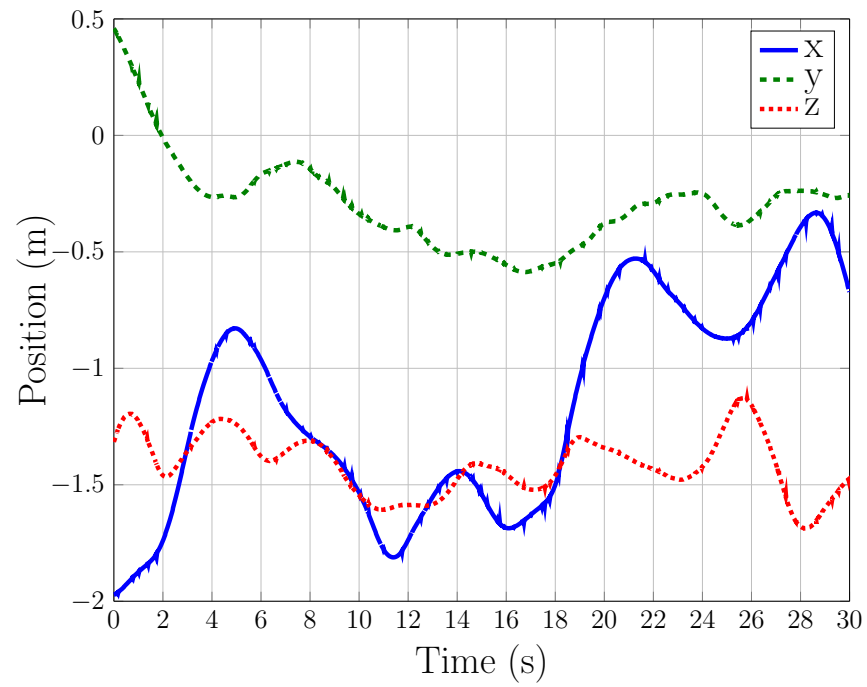


Figure 6.4: Motion Capture Position

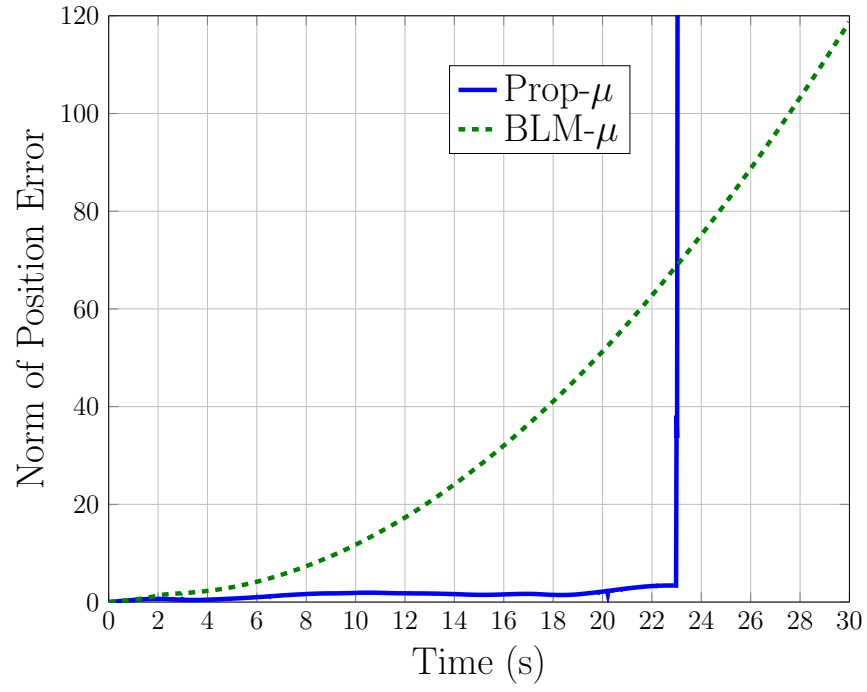


Figure 6.5: Error in Position of BLM- $\mu$  and Proposed- $\mu$  Estimator

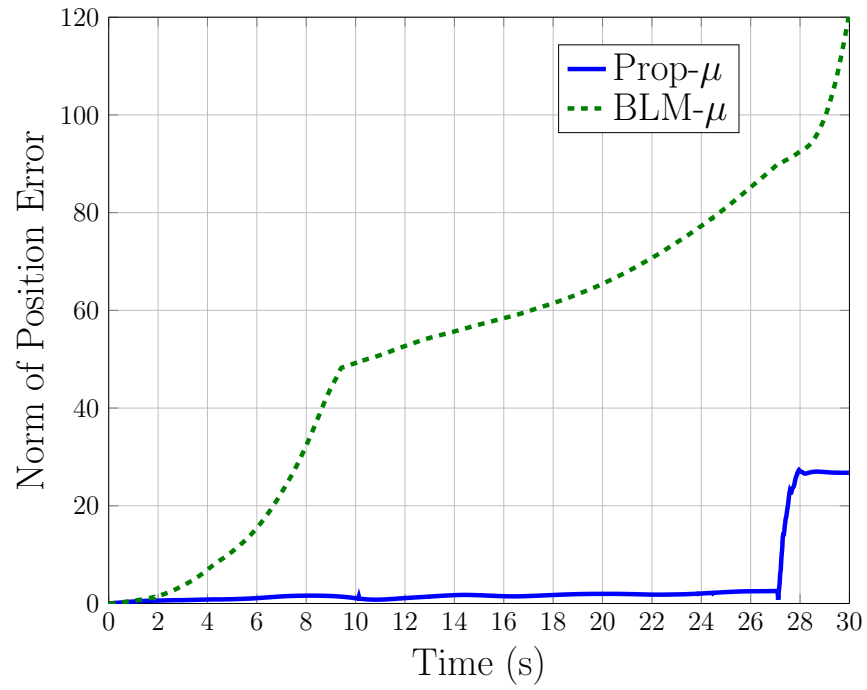


Figure 6.6: Case of Smaller Error in Position of Proposed- $\mu$  Compared with BLM- $\mu$  Estimator After 30 Seconds

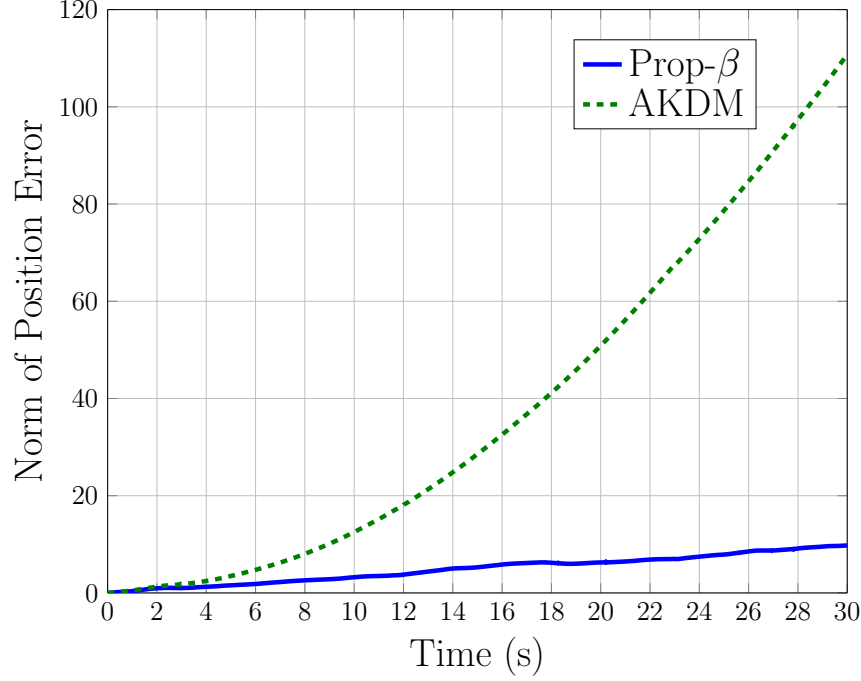


Figure 6.7: Error in Position of AKDM and Proposed- $\beta$  Estimator

error respectively over the trials, and Table 6.4 presents the standard deviation of the trials. First, note that the proposed and proposed- $\beta$  observers have both a lower average RMS error and standard deviation for the body frame z-axis velocity than the BLM, BLM- $\mu$ , and AKDM observers. Also, the maximum RMS error is lower for the proposed and proposed- $\beta$  observers than the minimum RMS error for the BLM, BLM- $\mu$ , and AKDM observers. This is due to the fact that including the Coriolis term in our model has enabled us to effectively estimate this additional state rather than using simple integration that is used in the BLM, BLM- $\mu$ , and AKDM observers.

By almost every metric, the proposed- $\mu$  estimator is by far the worst of the six estimators presented at observing the velocity vector. Note that this is due to the tendency of this proposed- $\mu$  observer to become unstable with respect to error. The median RMS error of the body frame z-axis velocity is only 0.2114 meters per second however. Again, this is lower than the minimum error shown for observers that do not leverage the Coriolis effect. It is not surprising that the proposed- $\mu$  observer had some unstable results. Figure 5.1 shows how this observer has consistently the worst local unobservability index of all the observers presented.

There is no clear improvement or harm produced by using the AKDM

Estimator	Roll Error	Pitch Error	$v_x^b$ Error	$v_y^b$ Error	$v_z^b$ Error
Proposed	0.120	0.083	0.351	0.384	0.169
BLM	0.143	0.0896	0.352	0.542	4.474
Proposed- $\mu$	0.119	0.109	$6.125 \times 10^{10}$	$1.106 \times 10^{13}$	$1.372 \times 10^8$
BLM- $\mu$	0.289	0.218	8.682	14.667	15.750
Proposed- $\beta$	0.126	0.083	0.348	0.396	0.171
AKDM	0.136	0.088	0.335	0.552	4.814

Table 6.1: Average RMS Error in Estimators

Estimator	Roll Error	Pitch Error	$v_x^b$ Error	$v_y^b$ Error	$v_z^b$ Error
Proposed	0.509	0.263	0.634	0.628	0.271
BLM	0.979	0.283	0.641	0.969	18.032
Proposed- $\mu$	0.778	1.068	$6.109 \times 10^{12}$	$1.106 \times 10^{15}$	$1.371 \times 10^{10}$
BLM- $\mu$	1.080	0.825	113.220	220.626	76.788
Proposed- $\beta$	0.519	0.236	0.623	0.572	0.276
AKDM	0.517	0.410	0.628	0.841	18.718

Table 6.2: Maximum RMS Error in Estimators

compared to the BLM or the proposed- $\beta$  compared to the proposed observers. With regard to several metrics (i.e. the velocity along the y-axis) these bias observing estimators do worse than their alternatives. However, the average RMS error of velocity along the x-axis is smallest for the AKDM observer. While the bias of low cost IMUs are high relative to higher grade sensors, these values are still typically small compared to the other states and angular velocities. This fact, along with the relatively high condition number of the AKDM and proposed- $\beta$  observers, make it difficult to accurately estimate the gyroscope bias.

Estimator	Roll Error	Pitch Error	$v_x^b$ Error	$v_y^b$ Error	$v_z^b$ Error
Proposed	0.034	0.027	0.147	0.243	0.095
BLM	0.035	0.025	0.119	0.337	0.662
Proposed- $\mu$	0.024	0.018	0.098	0.057	0.110
BLM- $\mu$	0.026	0.020	0.095	0.075	1.400
Proposed- $\beta$	0.035	0.026	0.140	0.251	0.095
AKDM	0.035	0.027	0.114	0.343	0.471

Table 6.3: Minimum RMS Error in Estimators

Estimator	Roll Error	Pitch Error	$v_x^b$ Error	$v_y^b$ Error	$v_z^b$ Error
Proposed	0.074	0.047	0.123	0.072	0.041
BLM	0.119	0.054	0.148	0.109	2.967
Proposed- $\mu$	0.108	0.141	$6.109 \times 10^{11}$	$1.106 \times 10^{14}$	$1.371 \times 10^9$
BLM- $\mu$	0.243	0.195	14.365	25.970	17.945
Proposed- $\beta$	0.073	0.046	0.124	0.074	0.042
AKDM	0.081	0.058	0.136	0.107	3.404

Table 6.4: Standard Deviation of RMS Error in Estimators

# CHAPTER 7

## CONCLUSIONS

In this thesis, we have presented an observer that leverages a model of a quadrotor and IMU data to compute roll, pitch, and the body frame velocity vector. The observer is able to effectively estimate one more state than previously presented observers. We have shown through analysis of the observability properties of the proposed observer and through flight tests that this observer will perform well over any reasonable flight condition. We have also shown, again through observability analysis and through flight tests, that it is ineffective to estimate either the H-force or gyroscope biases as part of our estimator. For low cost IMUs, we believe the proposed observer can substantially improve the performance of the inertial navigation capabilities of multirotor unmanned aircraft. This is immediately applicable in environments where the time between updated navigation data from an aiding sensor becomes longer or when the aiding sensor experiences a fault. In the future we shall explore integrating this method for inertial navigation with aiding sensors such as a monocular camera.

# APPENDIX A

## DETAILED RESULTS

This appendix presents the root mean square errors of five states - roll, pitch, and the three elements of the body frame velocity vector - produced by each of the six observers for each of the 110, thirty second trials. Each table presents results for a different observer. At the end of each table, the mean, standard deviation, minimum, and maximum result over all the trials are given for each state. Note that the proposed- $\mu$  observer occasionally produces results that run to infinity in finite time. In these cases, the trials are marked with a dash and are not included in the aggregated mean, standard deviation, minimum, or maximum result.

Trial	roll (rad)	pitch (rad)	$v_x$ (m/s)	$v_y$ (m/s)	$v_z$ (m/s)
1	0.160	0.052	0.164	0.409	2.291
2	0.040	0.052	0.247	0.457	4.814
3	0.059	0.102	0.234	0.506	4.535
4	0.282	0.410	0.555	0.523	11.171
5	0.043	0.039	0.195	0.526	4.640
6	0.126	0.044	0.243	0.589	3.353
7	0.045	0.036	0.204	0.581	4.232
8	0.049	0.036	0.292	0.525	4.118
9	0.047	0.037	0.195	0.561	4.415
10	0.051	0.036	0.281	0.571	4.067
11	0.081	0.047	0.293	0.470	3.683
12	0.048	0.050	0.133	0.407	4.122
13	0.041	0.034	0.163	0.406	4.634
14	0.043	0.038	0.165	0.433	4.574
15	0.047	0.036	0.162	0.467	4.624
16	0.050	0.027	0.206	0.500	4.290
17	0.084	0.068	0.259	0.566	4.198
18	0.036	0.029	0.133	0.459	4.233
19	0.055	0.039	0.216	0.513	4.408
20	0.058	0.043	0.397	0.503	4.409
21	0.053	0.052	0.166	0.348	4.326
22	0.040	0.041	0.226	0.398	4.367
23	0.051	0.039	0.183	0.491	4.131



24	0.066	0.132	0.212	0.523	2.761
25	0.065	0.033	0.171	0.537	4.563
26	0.151	0.160	0.399	0.718	3.177
27	0.147	0.088	0.439	0.527	0.471
28	0.070	0.121	0.235	0.503	3.282
29	0.179	0.121	0.438	0.642	1.561
30	0.282	0.154	0.551	0.756	12.905
31	0.096	0.058	0.315	0.411	2.994
32	0.104	0.121	0.315	0.372	2.536
33	0.079	0.058	0.344	0.415	3.853
34	0.094	0.064	0.256	0.486	3.909
35	0.173	0.098	0.421	0.626	2.537
36	0.198	0.125	0.444	0.632	6.883
37	0.161	0.076	0.493	0.536	1.135
38	0.177	0.129	0.490	0.662	4.942
39	0.162	0.080	0.332	0.505	1.674
40	0.080	0.050	0.235	0.491	2.662
41	0.069	0.054	0.243	0.490	3.852
42	0.165	0.132	0.453	0.593	1.992
43	0.165	0.092	0.401	0.617	1.067
44	0.269	0.196	0.508	0.782	18.718
45	0.121	0.050	0.200	0.454	3.370
46	0.068	0.050	0.262	0.463	3.453
47	0.051	0.048	0.224	0.446	4.757
48	0.097	0.073	0.287	0.464	2.936
49	0.083	0.069	0.218	0.525	3.212
50	0.137	0.076	0.347	0.533	3.198
51	0.220	0.122	0.455	0.691	10.167
52	0.147	0.147	0.398	0.561	4.536
53	0.153	0.078	0.295	0.535	0.939
54	0.113	0.050	0.236	0.426	3.375
55	0.077	0.050	0.309	0.494	3.713
56	0.069	0.111	0.363	0.543	2.827
57	0.173	0.095	0.435	0.603	2.428
58	0.266	0.120	0.516	0.755	11.066
59	0.237	0.115	0.421	0.708	6.882
60	0.236	0.151	0.550	0.755	12.521
61	0.231	0.101	0.539	0.647	9.112
62	0.227	0.163	0.596	0.686	12.372
63	0.239	0.051	0.203	0.515	2.024
64	0.051	0.034	0.175	0.424	4.525
65	0.047	0.035	0.133	0.442	4.422
66	0.035	0.041	0.123	0.453	4.218
67	0.125	0.046	0.186	0.478	3.401
68	0.053	0.028	0.246	0.505	4.256
69	0.145	0.089	0.396	0.619	2.563
70	0.221	0.114	0.533	0.595	8.637
71	0.517	0.045	0.114	0.374	4.692
72	0.146	0.066	0.369	0.548	1.771
73	0.218	0.114	0.475	0.811	5.483
74	0.187	0.296	0.493	0.578	6.589

75	0.187	0.085	0.526	0.605	2.029
76	0.173	0.066	0.431	0.636	1.589
77	0.108	0.070	0.332	0.561	2.041
78	0.076	0.032	0.213	0.516	4.408
79	0.210	0.142	0.494	0.689	4.760
80	0.240	0.136	0.521	0.808	9.763
81	0.236	0.077	0.470	0.719	7.715
82	0.087	0.061	0.226	0.414	3.477
83	0.301	0.065	0.357	0.638	6.071
84	0.242	0.078	0.441	0.677	11.546
85	0.091	0.066	0.269	0.438	2.476
86	0.100	0.071	0.340	0.522	2.280
87	0.140	0.139	0.352	0.584	1.004
88	0.244	0.114	0.538	0.661	9.205
89	0.049	0.039	0.140	0.343	4.704
90	0.172	0.078	0.418	0.595	1.009
91	0.215	0.057	0.325	0.540	3.243
92	0.162	0.094	0.481	0.672	1.567
93	0.160	0.113	0.429	0.620	1.877
94	0.112	0.068	0.353	0.545	1.983
95	0.171	0.103	0.355	0.648	2.055
96	0.163	0.173	0.514	0.606	9.113
97	0.124	0.047	0.209	0.459	2.661
98	0.039	0.027	0.136	0.438	4.430
99	0.068	0.044	0.201	0.444	4.389
100	0.052	0.118	0.211	0.481	3.251
101	0.108	0.034	0.170	0.514	4.018
102	0.158	0.166	0.355	0.523	3.043
103	0.214	0.181	0.579	0.654	8.031
104	0.217	0.097	0.527	0.610	9.093
105	0.198	0.227	0.567	0.841	13.035
106	0.267	0.213	0.628	0.661	18.012
107	0.228	0.073	0.489	0.611	9.460
108	0.206	0.133	0.493	0.681	7.313
109	0.116	0.068	0.367	0.571	3.157
110	0.128	0.130	0.339	0.545	1.180
mean	0.136	0.088	0.335	0.552	4.814
std	0.081	0.058	0.136	0.107	3.404
min	0.035	0.027	0.114	0.343	0.471
max	0.517	0.410	0.628	0.841	18.718

Table A.1: Detailed Results for AKDM Estimator

Trial	roll (rad)	pitch (rad)	$v_x$ (m/s)	$v_y$ (m/s)	$v_z$ (m/s)
1	0.352	0.197	7.808	10.447	8.158
2	0.028	0.042	0.247	0.125	5.103
3	0.067	0.161	1.579	0.754	4.661
4	0.691	0.341	11.937	59.990	26.670

5	0.031	0.028	0.223	0.158	4.865
6	0.357	0.213	7.462	22.540	14.348
7	0.031	0.026	0.255	0.187	4.417
8	0.046	0.041	0.400	0.729	4.011
9	0.034	0.031	0.135	0.363	4.581
10	0.039	0.027	0.291	0.120	4.438
11	0.047	0.041	0.392	0.233	4.367
12	0.043	0.051	0.137	0.100	4.254
13	0.032	0.024	0.123	0.104	4.832
14	0.100	0.061	1.705	4.671	3.365
15	0.030	0.028	0.199	0.113	4.809
16	0.048	0.038	0.562	1.551	4.214
17	0.051	0.042	0.413	0.253	4.599
18	0.029	0.024	0.143	0.075	4.377
19	0.041	0.028	0.261	0.138	4.647
20	0.129	0.081	1.313	6.945	2.497
21	0.035	0.037	0.187	0.128	4.677
22	0.087	0.089	1.475	3.964	2.958
23	0.095	0.069	1.013	4.051	3.202
24	0.471	0.265	4.883	30.634	18.626
25	0.045	0.024	0.188	0.132	4.823
26	0.254	0.297	7.841	8.038	8.643
27	0.270	0.274	10.661	13.807	8.818
28	0.310	0.348	10.267	20.894	10.595
29	0.497	0.377	15.059	17.112	16.669
30	0.776	0.548	30.188	28.452	65.463
31	0.070	0.047	0.450	0.157	3.973
32	0.751	0.611	36.675	68.783	56.857
33	0.205	0.224	4.567	4.540	4.547
34	0.061	0.055	0.278	0.182	4.352
35	0.436	0.272	9.133	21.557	23.034
36	0.582	0.352	11.426	25.475	33.221
37	0.114	0.068	0.591	0.176	2.576
38	0.561	0.791	52.330	62.755	49.341
39	0.217	0.241	8.598	12.110	6.983
40	0.246	0.134	4.099	13.106	4.894
41	0.105	0.093	1.685	3.853	2.666
42	0.405	0.306	0.852	14.711	17.770
43	0.113	0.078	0.502	0.155	2.352
44	0.593	0.577	30.677	54.501	50.454
45	0.340	0.191	10.698	20.029	6.616
46	0.046	0.036	0.311	0.155	3.926
47	0.037	0.034	0.319	0.107	5.005
48	0.062	0.058	0.438	0.239	4.100
49	0.321	0.248	4.861	12.941	13.178
50	0.093	0.058	0.362	0.150	4.021
51	0.594	0.433	14.232	13.799	24.002
52	0.384	0.328	12.314	25.694	20.692
53	0.707	0.185	7.110	34.305	21.149
54	0.157	0.071	0.691	2.244	2.014
55	0.115	0.104	1.573	3.106	2.258
56	0.388	0.393	15.963	28.054	16.396

57	0.129	0.073	0.532	0.247	4.973
58	0.518	0.480	15.304	12.738	41.843
59	0.389	0.324	9.766	8.584	19.951
60	0.368	0.283	6.919	10.434	18.007
61	0.495	0.589	24.522	18.121	48.135
62	0.573	0.349	10.684	17.233	25.851
63	1.080	0.326	24.448	95.522	69.207
64	0.038	0.024	0.148	0.108	4.791
65	0.032	0.029	0.108	0.092	4.737
66	0.026	0.030	0.095	0.113	4.457
67	0.334	0.156	4.600	27.236	10.100
68	0.037	0.020	0.274	0.187	4.458
69	0.094	0.074	0.445	0.334	3.914
70	0.565	0.825	113.220	220.626	57.461
71	0.507	0.036	0.184	0.139	4.770
72	0.322	0.262	9.179	9.345	11.881
73	0.381	0.270	6.457	9.539	19.321
74	0.299	0.239	4.612	6.917	8.783
75	0.190	0.172	4.082	3.626	3.083
76	0.205	0.241	7.024	6.772	4.972
77	0.263	0.281	7.005	9.914	10.416
78	0.061	0.026	0.180	0.158	4.606
79	0.341	0.289	7.852	12.876	15.555
80	0.707	0.493	41.140	45.140	49.592
81	0.811	0.690	29.846	37.254	76.788
82	0.239	0.215	5.925	11.146	6.240
83	0.734	0.470	18.226	25.012	43.531
84	0.653	0.317	17.326	37.404	34.253
85	0.298	0.181	2.567	8.535	5.290
86	0.074	0.052	0.509	0.279	3.532
87	0.532	0.379	15.078	19.367	26.866
88	0.594	0.459	20.272	11.838	33.876
89	0.090	0.049	0.802	3.488	4.008
90	0.123	0.066	0.515	0.320	2.380
91	0.546	0.267	12.017	29.483	28.221
92	0.351	0.294	9.543	12.416	14.066
93	0.160	0.091	0.542	2.088	1.573
94	0.221	0.203	6.696	8.739	5.731
95	0.124	0.082	0.428	0.168	1.401
96	0.363	0.524	17.381	14.946	26.828
97	0.470	0.235	11.299	34.278	25.888
98	0.031	0.020	0.173	0.125	4.562
99	0.067	0.048	0.381	1.067	4.266
100	0.493	0.254	5.293	38.547	16.262
101	0.336	0.119	3.753	10.407	3.723
102	0.200	0.200	1.810	7.504	3.213
103	0.517	0.579	26.157	20.339	44.589
104	0.802	0.483	35.135	31.197	48.680
105	0.275	0.204	0.768	6.610	8.834
106	0.763	0.632	23.925	26.259	67.230
107	0.340	0.333	14.896	10.699	24.556
108	0.657	0.692	26.348	27.839	54.642

109	0.083	0.056	0.205	0.177	4.009
110	0.099	0.058	0.327	0.117	2.568
mean	0.289	0.218	8.682	14.667	15.750
std	0.243	0.195	14.365	25.970	17.945
min	0.026	0.020	0.095	0.075	1.401
max	1.080	0.825	113.220	220.626	76.788

Table A.2: Detailed Results for BLM- $\mu$  Estimator

Trial	roll (rad)	pitch (rad)	$v_x$ (m/s)	$v_y$ (m/s)	$v_z$ (m/s)
1	0.118	0.050	0.176	0.357	3.481
2	0.044	0.058	0.247	0.459	4.818
3	0.054	0.086	0.238	0.509	4.631
4	0.102	0.190	0.285	0.539	2.240
5	0.039	0.037	0.197	0.525	4.741
6	0.095	0.058	0.247	0.583	3.907
7	0.039	0.035	0.207	0.581	4.308
8	0.041	0.033	0.290	0.524	4.234
9	0.045	0.037	0.203	0.560	4.507
10	0.047	0.037	0.282	0.571	4.230
11	0.067	0.048	0.307	0.458	4.106
12	0.059	0.057	0.144	0.410	4.045
13	0.040	0.031	0.165	0.416	4.716
14	0.035	0.033	0.163	0.430	4.711
15	0.039	0.036	0.167	0.471	4.704
16	0.044	0.030	0.214	0.493	4.432
17	0.058	0.053	0.265	0.555	4.464
18	0.037	0.032	0.141	0.461	4.268
19	0.050	0.035	0.214	0.510	4.502
20	0.057	0.043	0.402	0.499	4.577
21	0.051	0.048	0.166	0.350	4.484
22	0.040	0.036	0.227	0.393	4.501
23	0.044	0.037	0.187	0.486	4.298
24	0.050	0.094	0.164	0.525	3.794
25	0.057	0.033	0.177	0.536	4.703
26	0.159	0.149	0.383	0.722	1.733
27	0.134	0.089	0.472	0.503	1.468
28	0.069	0.093	0.243	0.500	3.892
29	0.187	0.103	0.471	0.632	1.146
30	0.275	0.160	0.565	0.726	10.520
31	0.095	0.058	0.333	0.400	3.378
32	0.108	0.098	0.324	0.374	3.047
33	0.068	0.075	0.363	0.405	3.850
34	0.099	0.068	0.268	0.483	4.080
35	0.196	0.093	0.448	0.637	1.741
36	0.235	0.162	0.475	0.623	6.855
37	0.175	0.086	0.537	0.516	1.393
38	0.247	0.167	0.565	0.728	7.628
39	0.156	0.084	0.374	0.487	1.039

40	0.102	0.051	0.241	0.506	2.470
41	0.063	0.057	0.251	0.479	4.120
42	0.152	0.131	0.461	0.588	0.662
43	0.168	0.105	0.442	0.599	0.881
44	0.290	0.193	0.551	0.787	14.695
45	0.098	0.048	0.217	0.431	3.934
46	0.054	0.045	0.260	0.457	3.762
47	0.047	0.044	0.225	0.440	4.867
48	0.088	0.083	0.293	0.453	3.324
49	0.087	0.233	0.378	0.523	3.844
50	0.155	0.081	0.386	0.545	3.396
51	0.257	0.127	0.472	0.707	9.415
52	0.167	0.163	0.409	0.575	4.822
53	0.170	0.087	0.334	0.558	1.543
54	0.082	0.041	0.229	0.406	4.141
55	0.071	0.050	0.321	0.482	4.103
56	0.065	0.084	0.333	0.534	3.530
57	0.178	0.099	0.472	0.592	2.464
58	0.259	0.137	0.580	0.705	7.940
59	0.223	0.121	0.464	0.656	3.772
60	0.256	0.150	0.571	0.748	10.144
61	0.229	0.128	0.600	0.578	6.184
62	0.255	0.186	0.621	0.697	11.848
63	0.160	0.043	0.222	0.421	2.286
64	0.048	0.032	0.182	0.426	4.650
65	0.047	0.037	0.140	0.440	4.545
66	0.035	0.037	0.119	0.453	4.317
67	0.084	0.038	0.181	0.476	4.352
68	0.043	0.027	0.252	0.506	4.381
69	0.135	0.095	0.419	0.604	3.156
70	0.240	0.149	0.581	0.583	7.688
71	0.508	0.036	0.122	0.372	4.861
72	0.122	0.059	0.391	0.509	2.676
73	0.222	0.122	0.516	0.784	3.139
74	0.218	0.247	0.458	0.607	5.178
75	0.184	0.102	0.564	0.564	1.445
76	0.176	0.084	0.461	0.596	1.258
77	0.104	0.069	0.348	0.556	2.634
78	0.079	0.040	0.231	0.517	4.473
79	0.208	0.132	0.525	0.650	2.674
80	0.300	0.146	0.578	0.826	8.984
81	0.233	0.100	0.519	0.657	5.852
82	0.080	0.053	0.244	0.406	4.121
83	0.232	0.075	0.382	0.571	1.757
84	0.262	0.100	0.496	0.656	9.962
85	0.090	0.097	0.282	0.429	2.546
86	0.979	0.070	0.351	0.516	2.812
87	0.141	0.126	0.366	0.558	1.275
88	0.249	0.134	0.599	0.625	7.556
89	0.041	0.033	0.148	0.337	4.838
90	0.162	0.086	0.453	0.551	1.343

91	0.176	0.053	0.337	0.503	1.459
92	0.156	0.106	0.509	0.643	1.082
93	0.162	0.111	0.442	0.608	0.942
94	0.104	0.070	0.371	0.526	2.618
95	0.201	0.101	0.395	0.660	1.904
96	0.166	0.178	0.512	0.596	6.266
97	0.087	0.041	0.207	0.424	3.706
98	0.036	0.025	0.139	0.442	4.507
99	0.051	0.053	0.205	0.436	4.549
100	0.035	0.089	0.178	0.482	3.904
101	0.087	0.043	0.171	0.508	4.197
102	0.164	0.159	0.370	0.514	2.205
103	0.240	0.190	0.595	0.619	5.631
104	0.231	0.109	0.563	0.568	7.915
105	0.348	0.283	0.613	0.969	18.032
106	0.268	0.227	0.641	0.639	16.258
107	0.230	0.099	0.549	0.549	6.986
108	0.232	0.154	0.545	0.678	6.530
109	0.157	0.086	0.426	0.611	2.757
110	0.129	0.122	0.367	0.516	0.915
mean	0.143	0.090	0.352	0.542	4.474
std	0.119	0.054	0.148	0.109	2.967
min	0.035	0.025	0.119	0.337	0.662
max	0.979	0.283	0.641	0.969	18.032

Table A.3: Detailed Results for BLM Estimator

Trial	roll (rad)	pitch (rad)	$v_x$ (m/s)	$v_y$ (m/s)	$v_z$ (m/s)
1	0.157	0.050	0.197	0.318	0.179
2	0.039	0.052	0.260	0.303	0.187
3	0.059	0.104	0.260	0.353	0.106
4	0.099	0.122	0.211	0.363	0.198
5	0.056	0.039	0.228	0.363	0.119
6	0.125	0.051	0.264	0.427	0.205
7	0.048	0.035	0.269	0.397	0.178
8	0.049	0.034	0.328	0.344	0.117
9	0.047	0.040	0.188	0.381	0.114
10	0.052	0.030	0.271	0.401	0.176
11	0.075	0.048	0.305	0.338	0.220
12	0.058	0.053	0.146	0.277	0.138
13	0.041	0.033	0.166	0.265	0.125
14	0.043	0.037	0.157	0.309	0.112
15	0.047	0.034	0.190	0.319	0.104
16	0.051	0.029	0.204	0.338	0.122
17	0.075	0.053	0.311	0.390	0.114
18	0.039	0.030	0.140	0.309	0.095
19	0.056	0.036	0.226	0.362	0.129

20	0.058	0.044	0.438	0.344	0.115
21	0.051	0.053	0.196	0.251	0.165
22	0.040	0.039	0.244	0.295	0.108
23	0.051	0.039	0.202	0.364	0.127
24	0.056	0.133	0.248	0.344	0.140
25	0.064	0.037	0.242	0.363	0.135
26	0.129	0.157	0.467	0.482	0.142
27	0.135	0.084	0.499	0.377	0.182
28	0.068	0.117	0.288	0.345	0.098
29	0.167	0.149	0.469	0.441	0.176
30	0.256	0.153	0.565	0.515	0.204
31	0.092	0.056	0.363	0.331	0.204
32	0.099	0.167	0.367	0.267	0.144
33	0.082	0.060	0.377	0.338	0.155
34	0.082	0.064	0.285	0.326	0.123
35	0.154	0.099	0.419	0.416	0.211
36	0.180	0.125	0.476	0.477	0.225
37	0.151	0.075	0.510	0.408	0.214
38	0.161	0.121	0.436	0.442	0.257
39	0.135	0.074	0.383	0.330	0.237
40	0.072	0.052	0.290	0.336	0.144
41	0.070	0.052	0.287	0.366	0.168
42	0.156	0.121	0.498	0.436	0.172
43	0.153	0.087	0.417	0.423	0.217
44	0.225	0.182	0.473	0.563	0.190
45	0.121	0.047	0.252	0.372	0.195
46	0.068	0.048	0.319	0.350	0.146
47	0.051	0.046	0.243	0.324	0.117
48	0.103	0.074	0.335	0.379	0.144
49	0.081	0.066	0.268	0.399	0.162
50	0.126	0.074	0.342	0.375	0.200
51	0.200	0.116	0.420	0.453	0.195
52	0.138	0.134	0.364	0.448	0.199
53	0.145	0.079	0.240	0.364	0.117
54	0.107	0.051	0.262	0.325	0.159
55	0.076	0.047	0.333	0.368	0.129
56	0.068	0.104	0.395	0.400	0.156
57	0.165	0.092	0.435	0.460	0.187
58	0.228	0.117	0.487	0.421	0.197
59	0.210	0.116	0.486	0.484	0.155
60	0.209	0.138	0.541	0.511	0.221
61	0.223	0.091	0.484	0.487	0.212
62	0.211	0.153	0.601	0.517	0.239
63	0.215	0.050	0.269	0.389	0.205
64	0.051	0.037	0.190	0.318	0.200
65	0.047	0.034	0.159	0.334	0.129
66	0.035	0.040	0.156	0.334	0.115
67	0.124	0.044	0.223	0.352	0.131
68	0.055	0.027	0.282	0.369	0.145
69	0.131	0.088	0.429	0.443	0.188
70	0.214	0.106	0.476	0.479	0.210



71	0.519	0.056	0.146	0.270	0.172
72	0.142	0.060	0.443	0.409	0.218
73	0.185	0.123	0.623	0.528	0.209
74	0.157	0.236	0.456	0.406	0.202
75	0.192	0.071	0.512	0.528	0.214
76	0.159	0.062	0.465	0.463	0.222
77	0.101	0.069	0.385	0.400	0.228
78	0.074	0.033	0.221	0.375	0.115
79	0.198	0.135	0.450	0.530	0.180
80	0.216	0.131	0.443	0.526	0.236
81	0.206	0.070	0.480	0.472	0.276
82	0.078	0.053	0.237	0.288	0.201
83	0.250	0.065	0.361	0.430	0.195
84	0.219	0.076	0.428	0.482	0.221
85	0.084	0.055	0.274	0.304	0.168
86	0.095	0.066	0.403	0.419	0.147
87	0.131	0.134	0.336	0.422	0.153
88	0.231	0.111	0.526	0.502	0.173
89	0.049	0.039	0.167	0.253	0.139
90	0.160	0.075	0.429	0.478	0.172
91	0.206	0.057	0.326	0.397	0.153
92	0.148	0.091	0.501	0.448	0.157
93	0.144	0.113	0.471	0.453	0.146
94	0.106	0.063	0.377	0.386	0.151
95	0.157	0.098	0.386	0.442	0.174
96	0.158	0.166	0.496	0.503	0.165
97	0.120	0.047	0.236	0.380	0.170
98	0.040	0.026	0.188	0.306	0.103
99	0.068	0.048	0.244	0.322	0.134
100	0.070	0.125	0.210	0.342	0.101
101	0.128	0.096	0.210	0.356	0.114
102	0.141	0.163	0.401	0.379	0.205
103	0.197	0.164	0.533	0.486	0.239
104	0.197	0.094	0.537	0.469	0.208
105	0.167	0.226	0.522	0.572	0.201
106	0.243	0.199	0.601	0.516	0.187
107	0.215	0.065	0.449	0.491	0.224
108	0.189	0.129	0.453	0.499	0.258
109	0.104	0.070	0.260	0.367	0.220
110	0.129	0.131	0.347	0.385	0.167
mean	0.126	0.083	0.348	0.396	0.171
std	0.073	0.046	0.124	0.074	0.042
min	0.035	0.026	0.140	0.251	0.095
max	0.519	0.236	0.623	0.572	0.276

Table A.4: Detailed Results for Proposed- $\beta$  Estimator

Trial	roll (rad)	pitch (rad)	$v_x$ (m/s)	$v_y$ (m/s)	$v_z$ (m/s)
1	0.171	0.526	6.110E+12	1.110E+15	1.370E+10
2	0.027	0.040	0.250	0.121	0.196
3	0.151	0.168	4.356	3.855	13.825
4	0.067	0.127	0.260	0.142	0.215
5	0.029	0.026	0.224	0.098	0.116
6	-	-	-	-	-
7	0.030	0.025	0.275	0.127	0.201
8	0.033	0.026	0.342	0.093	0.133
9	0.029	0.030	0.120	0.096	0.126
10	0.038	0.026	0.293	0.092	0.191
11	0.045	0.041	0.401	0.224	0.242
12	0.189	0.171	0.448	1.179	2.743
13	0.030	0.022	0.120	0.064	0.136
14	0.024	0.026	0.145	0.072	0.127
15	0.028	0.026	0.205	0.074	0.120
16	0.033	0.022	0.206	0.068	0.129
17	0.412	0.532	22.733	31.363	3.390E+03
18	0.028	0.023	0.149	0.057	0.116
19	-	-	-	-	-
20	0.043	0.030	0.454	0.142	0.141
21	0.032	0.035	0.200	0.105	0.183
22	0.032	0.028	0.254	0.086	0.118
23	0.034	0.028	0.248	0.126	0.134
24	0.037	0.081	0.193	0.109	0.144
25	0.042	0.023	0.196	0.083	0.148
26	0.095	0.123	0.437	0.312	0.148
27	0.097	0.063	0.630	0.202	0.208
28	0.045	0.090	0.301	0.128	0.110
29	0.122	0.102	0.529	0.169	0.174
30	-	-	-	-	-
31	0.068	0.046	0.458	0.134	0.214
32	0.064	0.111	0.407	0.171	0.163
33	0.049	0.060	0.452	0.219	0.192
34	0.058	0.055	0.278	0.088	0.132
35	0.120	0.102	0.441	0.264	0.247
36	0.423	0.656	5.337	5.541	333.382
37	0.114	0.070	0.599	0.166	0.221
38	0.139	0.114	0.388	0.142	0.310
39	0.105	0.068	0.576	0.232	0.273
40	0.065	0.053	0.271	0.083	0.162
41	0.049	0.043	0.299	0.136	0.180
42	0.108	0.091	0.594	0.258	0.174
43	0.114	0.079	0.509	0.140	0.242
44	0.778	1.068	75.194	53.549	2.770E+03
45	0.070	0.037	0.383	0.136	0.222
46	0.041	0.035	0.327	0.145	0.159
47	0.035	0.032	0.340	0.089	0.132
48	0.177	0.133	0.456	0.274	10.452
49	0.087	0.091	0.354	0.206	0.184

50	0.097	0.062	0.365	0.137	0.232
51	0.173	0.143	0.466	0.281	0.231
52	0.105	0.120	0.339	0.229	0.229
53	0.104	0.072	0.194	0.080	0.148
54	0.084	0.038	0.270	0.228	0.188
55	0.053	0.038	0.359	0.118	0.146
56	0.053	0.077	0.490	0.221	0.166
57	0.129	0.074	0.543	0.248	0.204
58	-	-	-	-	-
59	-	-	-	-	-
60	0.205	0.180	0.727	0.377	0.282
61	0.178	0.077	0.598	0.168	0.238
62	0.182	0.171	0.722	0.333	0.307
63	-	-	-	-	-
64	0.035	0.022	0.149	0.066	0.211
65	0.031	0.027	0.107	0.063	0.148
66	0.025	0.028	0.098	0.081	0.128
67	0.130	0.075	0.391	0.648	0.227
68	0.035	0.018	0.278	0.100	0.156
69	0.094	0.074	0.459	0.323	0.212
70	0.184	0.093	0.408	0.208	0.249
71	0.505	0.039	0.201	0.106	0.469
72	0.084	0.046	0.622	0.183	0.250
73	0.142	0.150	0.738	0.440	0.241
74	0.137	0.188	0.586	0.284	0.252
75	0.153	0.064	0.616	0.218	0.248
76	0.129	0.047	0.537	0.217	0.271
77	0.077	0.055	0.473	0.178	0.238
78	0.063	0.027	0.185	0.133	0.147
79	0.152	0.103	0.538	0.240	0.209
80	0.201	0.144	0.531	0.269	0.286
81	0.175	0.086	0.540	0.248	0.337
82	0.116	0.192	0.495	0.167	0.232
83	-	-	-	-	-
84	0.214	0.136	0.601	0.330	0.264
85	0.061	0.039	0.288	0.110	0.186
86	0.073	0.052	0.514	0.276	0.174
87	0.091	0.098	0.377	0.244	0.169
88	-	-	-	-	-
89	0.234	0.261	2.688	2.783	1.152
90	0.121	0.068	0.535	0.312	0.179
91	-	-	-	-	-
92	0.111	0.080	0.539	0.237	0.187
93	0.110	0.090	0.525	0.209	0.172
94	0.078	0.050	0.453	0.216	0.169
95	0.127	0.086	0.437	0.162	0.213
96	0.247	0.257	1.178	1.592	0.558
97	0.142	0.140	0.428	0.251	0.677
98	-	-	-	-	-
99	0.054	0.068	0.246	0.166	0.146

100	0.287	0.286	1.600E+10	7.460E+09	4.160E+06
101	0.154	0.132	2.785	3.121	8.376
102	0.103	0.120	0.370	0.201	0.220
103	0.155	0.129	0.557	0.237	0.297
104	0.170	0.081	0.543	0.277	0.267
105	0.150	0.222	0.320	0.182	0.267
106	0.235	0.243	0.739	0.434	0.242
107	0.179	0.060	0.497	0.294	0.255
108	0.155	0.104	0.403	0.191	0.350
109	0.094	0.069	0.289	0.242	0.313
110	0.109	0.072	0.331	0.125	0.187
mean	0.119	0.109	61248480002	1.106E+13	137171687
std	0.107	0.141	6.109E+11	1.106E+14	1371295852
min	0.024	0.018	0.098	0.057	0.110
max	0.778	1.068	6.109E+12	1.106E+15	13713000000

Table A.5: Detailed Results for Proposed- $\mu$  Estimator

Trial	roll (rad)	pitch (rad)	$v_x$ (m/s)	$v_y$ (m/s)	$v_z$ (m/s)
1	0.115	0.048	0.208	0.271	0.172
2	0.041	0.057	0.256	0.303	0.187
3	0.041	0.088	0.263	0.351	0.104
4	0.100	0.060	0.191	0.368	0.197
5	0.038	0.037	0.227	0.356	0.116
6	0.116	0.054	0.270	0.418	0.211
7	0.041	0.038	0.273	0.393	0.177
8	0.039	0.034	0.327	0.339	0.119
9	0.043	0.045	0.198	0.376	0.115
10	0.047	0.031	0.275	0.397	0.177
11	0.060	0.048	0.312	0.332	0.218
12	0.050	0.046	0.154	0.276	0.140
13	0.039	0.031	0.170	0.270	0.126
14	0.034	0.032	0.158	0.304	0.112
15	0.038	0.033	0.197	0.316	0.104
16	0.042	0.033	0.209	0.325	0.122
17	0.078	0.084	0.320	0.382	0.115
18	0.037	0.036	0.149	0.304	0.095
19	0.058	0.032	0.231	0.364	0.130
20	0.056	0.046	0.443	0.338	0.116
21	0.047	0.049	0.196	0.252	0.165
22	0.041	0.033	0.244	0.289	0.108
23	0.044	0.037	0.210	0.355	0.127
24	0.050	0.104	0.214	0.343	0.139
25	0.055	0.041	0.242	0.360	0.135
26	0.126	0.146	0.436	0.498	0.135
27	0.120	0.086	0.507	0.369	0.183
28	0.061	0.091	0.297	0.336	0.096
29	0.164	0.111	0.489	0.434	0.167
30	0.235	0.175	0.507	0.475	0.190

31	0.089	0.057	0.370	0.317	0.201
32	0.091	0.063	0.354	0.270	0.149
33	0.066	0.066	0.386	0.326	0.155
34	0.081	0.066	0.284	0.319	0.123
35	0.154	0.101	0.416	0.414	0.211
36	0.184	0.155	0.462	0.462	0.238
37	0.148	0.076	0.532	0.360	0.213
38	0.195	0.139	0.461	0.466	0.258
39	0.130	0.077	0.402	0.354	0.236
40	0.079	0.056	0.285	0.329	0.144
41	0.062	0.052	0.290	0.348	0.168
42	0.135	0.116	0.503	0.438	0.172
43	0.145	0.092	0.429	0.386	0.216
44	0.227	0.188	0.495	0.536	0.178
45	0.097	0.046	0.268	0.347	0.195
46	0.053	0.044	0.319	0.340	0.144
47	0.046	0.040	0.243	0.313	0.116
48	0.092	0.086	0.336	0.358	0.144
49	0.085	0.166	0.362	0.399	0.182
50	0.119	0.069	0.357	0.354	0.199
51	0.209	0.129	0.390	0.427	0.196
52	0.156	0.148	0.366	0.466	0.201
53	0.144	0.081	0.250	0.350	0.117
54	0.077	0.044	0.256	0.307	0.161
55	0.068	0.046	0.343	0.352	0.129
56	0.063	0.078	0.373	0.385	0.155
57	0.162	0.091	0.455	0.438	0.183
58	0.221	0.120	0.510	0.439	0.196
59	0.187	0.123	0.479	0.455	0.147
60	0.207	0.149	0.513	0.495	0.214
61	0.223	0.102	0.501	0.477	0.212
62	0.222	0.167	0.575	0.505	0.231
63	0.161	0.045	0.275	0.342	0.202
64	0.045	0.035	0.192	0.312	0.199
65	0.044	0.035	0.164	0.324	0.129
66	0.034	0.036	0.155	0.329	0.116
67	0.081	0.036	0.226	0.337	0.134
68	0.043	0.028	0.290	0.359	0.146
69	0.119	0.094	0.428	0.432	0.182
70	0.226	0.131	0.495	0.461	0.210
71	0.509	0.046	0.147	0.265	0.171
72	0.117	0.055	0.461	0.380	0.218
73	0.176	0.135	0.601	0.525	0.205
74	0.167	0.134	0.394	0.382	0.168
75	0.187	0.081	0.537	0.480	0.203
76	0.155	0.062	0.451	0.424	0.217
77	0.094	0.065	0.382	0.398	0.224
78	0.078	0.036	0.223	0.382	0.118
79	0.191	0.113	0.461	0.480	0.173

80	0.231	0.149	0.449	0.456	0.231
81	0.193	0.090	0.492	0.440	0.271
82	0.069	0.056	0.251	0.282	0.204
83	0.202	0.073	0.361	0.420	0.194
84	0.221	0.096	0.429	0.434	0.209
85	0.076	0.069	0.283	0.293	0.168
86	0.090	0.067	0.414	0.415	0.145
87	0.124	0.127	0.350	0.400	0.148
88	0.223	0.129	0.549	0.452	0.170
89	0.039	0.032	0.174	0.243	0.139
90	0.147	0.075	0.423	0.449	0.170
91	0.163	0.046	0.317	0.356	0.144
92	0.139	0.099	0.509	0.430	0.158
93	0.138	0.112	0.465	0.433	0.146
94	0.095	0.062	0.388	0.370	0.150
95	0.167	0.100	0.401	0.423	0.176
96	0.159	0.155	0.463	0.514	0.152
97	0.088	0.042	0.232	0.347	0.173
98	0.060	0.027	0.191	0.349	0.104
99	0.074	0.069	0.251	0.307	0.152
100	0.048	0.086	0.194	0.342	0.103
101	0.092	0.061	0.215	0.354	0.112
102	0.142	0.156	0.393	0.377	0.195
103	0.198	0.162	0.518	0.471	0.236
104	0.196	0.095	0.519	0.427	0.207
105	0.238	0.263	0.527	0.628	0.207
106	0.245	0.247	0.634	0.535	0.190
107	0.214	0.073	0.458	0.467	0.220
108	0.202	0.135	0.464	0.498	0.258
109	0.131	0.068	0.277	0.378	0.225
110	0.119	0.088	0.354	0.349	0.156
mean	0.120	0.083	0.351	0.384	0.169
std	0.074	0.047	0.123	0.072	0.041
min	0.034	0.027	0.147	0.243	0.095
max	0.509	0.263	0.634	0.628	0.271

Table A.6: Detailed Results for Proposed Estimator

## REFERENCES

- [1] D. Titterton and J. Weston, *Strapdown Inertial Navigation Technology*, 2nd ed., ser. Radar, Sonar, Navigation and Avionics Series, N. Stewart and H. Griffiths, Eds. The Institution and Engineering and Technology, 2004, vol. 17.
- [2] P. G. Savage, “Strapdown inertial navigation integration algorithm design part 1: Attitude algorithms,” *Journal of Guidance, Control, and Dynamics*, vol. 21, no. 1, pp. 19–28, January 1998.
- [3] P. G. Savage, “Strapdown inertial navigation integration algorithm design part 2: Velocity and position algorithms,” *Journal of Guidance, Control, and Dynamics*, vol. 21, no. 2, pp. 208–221, March 1998.
- [4] P. G. Savage, “A unified mathematical framework for strapdown algorithm design,” *Journal of Guidance, Control, and Dynamics*, vol. 29, no. 2, pp. 237–249, March 2006.
- [5] Y. A. Litmanovich, V. M. Lesyuchevsky, and V. Z. Gusinsky, “Two new classes of strapdown navigation algorithms,” *Journal of Guidance, Control, and Dynamics*, vol. 23, no. 1, pp. 34–44, January 2000.
- [6] M. B. Ignagni, “Optimal strapdown attitude integration algorithms,” *Journal of Guidance, Control, and Dynamics*, vol. 13, no. 2, pp. 363–369, March 1990.
- [7] P. G. Savage, “Explicit frequency-shaped coning algorithms for pseudoconing environments,” *Journal of Guidance, Control, and Dynamics*, vol. 34, no. 3, pp. 774–782, May 2011.
- [8] P. G. Savage, “Coning algorithm design by explicit frequency shaping,” *Journal of Guidance, Control, and Dynamics*, vol. 33, no. 4, pp. 1123–1132, July 2010.
- [9] P. G. Savage, “Strapdown sculling algorithm design for sensor dynamic amplitude and phase-shift error,” *Journal of Guidance, Control, and Dynamics*, vol. 35, no. 6, pp. 1718–1729, November 2012.

- [10] H. Chao, C. Coopmans, L. Di, and Y. Q. Chen, “A comparative evaluation of low-cost imu for unmanned autonomous systems,” in *Proceedings of the IEEE International Conference on Multisensor Fusion and Integration for Intelligent Systems*, Salt Lake City, Utah, September 2010, pp. 211–216.
- [11] H. Zhao and Z. Wang, “Motion measurement using inertial sensors, ultrasonic sensors, and magnetometers with extended kalman filter for data fusion,” *IEEE Sensors Journal*, vol. 12, no. 5, pp. 943–953, May 2012.
- [12] I. Sa and P. Corke, “System identification, estimation and control for a cost effective open-source quadcopter,” in *IEEE International Conference on Robotics and Automation*, RiverCentre, Saint Paul, Minnesota, USA, May 2012, pp. 2202–2209.
- [13] S. Grzonka, G. Grisetti, and W. Burgard, “Towards a navigation system for autonomous indoor flying,” in *IEEE International Conference on Robotics and Automation*, Kobe International Conference Center, Kobe, Japan, May 2009, pp. 2878–2883.
- [14] D. B. Kingston and R. W. Beard, “Real-time attitude and position estimation for small uavs using low-cost sensors,” in *AIAA “Unmanned Unlimited” Technical Conference, Workshop and Exhibit*, Chicago, Illinois, September 2004.
- [15] M. Tailanian, S. Paternain, R. Rosa, and R. Canetti, “Design and implementation of sensor data fusion for an autonomous quadrotor,” in *IEEE Instrumentation and Measurement Technology Conference*, Montevideo, Uruguay, May 2014, pp. 1431–1436.
- [16] D. Scaramuzza, M. C. Achtelik, L. Doitsidis, F. Fraundorfer, E. Kosmatopoulos, A. Martinelli, M. W. Achtelik, M. Chli, S. Chatzichristofis, L. Kneip, D. Gurdan, L. Heng, G. H. Lee, S. Lynen, L. Meier, M. Pollefeys, A. Renzaglia, R. Siegwart, J. C. Stumpf, P. Tanskanen, C. Troiani, and S. Weiss, “Vision-controlled micro flying robots: From system design to autonomous navigation and mapping in gps-denied environments,” *IEEE Robotics and Automation Magazine*, pp. 26–40, September 2014.
- [17] D. M. W. Abeywardena and S. R. Munasinghe, “Performance analysis of a kalman filter based attitude estimator for a quad rotor uav,” in *IEEE International Congress on Ultra Modern Telecommunications and Control Systems Workshops*, Moscow, Russia, October 2010, pp. 466–471.



- [18] D. Abeywardena, S. Kodagoda, G. Dissanayake, and R. Munasinghe, “Improved state estimation in quadrotor mavs,” *IEEE Robotics and Automation Magazine*, 2013.
- [19] R. C. Leishman, J. C. MacDonald, R. W. Beard, and T. W. McLain, “Quadrotors and accelerometers: State estimation with an improved dynamic model,” *IEEE Control Systems Magazine*, 2014.
- [20] J. Macdonald, R. Leishman, R. Beard, and T. McLain, “Analysis of an improved imu-based observer for multirotor helicopters,” *Journal of Intelligent and Robotic Systems*, 2014.
- [21] R. Sanz, L. Rodenas, P. Garcia, and P. Castillo, “Improving attitude estimation using inertial sensors for quadrotor control systems,” in *International Conference on Unmanned Aircraft Systems*, Orlando, Florida, May 2014, pp. 895–901.
- [22] P. Martin and E. Salaun, “The true role of accelerometer feedback in quadrotor control,” in *IEEE International Conference on Robotics and Automation*.
- [23] R. Baranek and F. Solc, “Model-based attitude estimation for multi-copters,” *Advances in Electrical and Electronic Engineering*, 2014.
- [24] D. L. Guimares, “Ascending technologies pelican cad model,” <http://wiki.asctec.de/display/AR/CAD+Models>.
- [25] D. T. Greenwood, *Principles of Dynamics*, 2nd ed. Upper Saddle River, NJ: Prentice Hall, 1988.
- [26] S. Bouabdallah, P. Murrieri, and R. Siegwart, “Design and control of an indoor micro quadrotor,” in *Proceedings of the IEEE International Conference on Robotics and Automation*, New Orleans, LA, April 2004, pp. 4393–4398.
- [27] S. Bouabdallah and R. Siegwart, “Full control of a quadrotor,” in *Proceedings of the IEEE/RSJ International Conference on Intelligent Robots and Systems*, San Diego, CA, October 2007, pp. 153–158.
- [28] L. Derafa, T. Madani, and A. Benallegue, “Dynamic modelling and experimental identification of four rotors helicopter parameters,” in *IEEE Conference on Industrial Technology*, Mumbai, India, December 2006, pp. 1834–1839.
- [29] M. Bangura and R. Mahony, “Nonlinear dynamic modeling for high performance control of a quadrotor,” in *Proceedings of Australasian Conference on Robotics and Automation*, Victoria University of Wellington, New Zealand, December 2012.

- [30] P. J. Bristeau, P. Martin, E. Salaun, and N. Petit, “The role of propeller aerodynamics in the model of a quadrotor uav,” in *Proceedings of the European Control Conference*, Budapest, Hungary, August 2009, pp. 683–688.
- [31] R. Mahony, V. Kumar, and P. Corke, “Multirotor aerial vehicles: Modeling, estimation, and control of quadrotor,” *IEEE Robotics and Automation Magazine*, pp. 20–32, September 2012.
- [32] G. M. Hoffmann, H. Huang, S. L. Waslander, and C. J. Tomlin, “Quadrotor helicopter flight dynamics and control: Theory and experiment,” in *AIAA Guidance, Navigation and Control Conference and Exhibit*, Hilton Head, South Carolina, August 2007.
- [33] S. Sukkarieh, P. Gibbens, B. Grocholsky, K. Willis, and H. F. Durrant-Whyte, “A low-cost, redundant inertial measurement unit for unmanned air vehicles,” *International Journal of Robotics Research*, vol. 19, no. 11, pp. 1089–1103, November 2000.
- [34] S. Thrun, W. Burgard, and D. Fox, *Probabilistic Robots*, ser. Intelligent Robotics and Autonomous Agents Series. MIT Press, 2006.
- [35] A. J. Krener and K. Ide, “Measures of unobservability,” in *Proceedings of the 48th IEEE Conference on Decision and Control*, Shanghai, December 2009.
- [36] J. Hernandez, K. Tsotos, and S. Soatto, “Observability, identifiability and sensitivity of vision-aided inertial navigation,” in *Proceedings of the International Conference on Robotics and Automation (ICRA)*, May 2015.
- [37] R. Hermann and A. J. Krener, “Nonlinear controllability and observability,” *IEEE Transactions on Automatic Control*, vol. 22, pp. 728–740, 1977.
- [38] W. Kang, A. J. Krener, M. Xiao, and L. Xu, *Data Assimilation for Atmospheric, Oceanic and Hydrologic Applications*. Springer, February 2013, vol. 2, ch. 1: A Survey of Observers for Nonlinear Dynamical Systems, pp. 1–25.